moniliforme, *Eurotium*, *Aspergillus fumigatus*, *Curvularis*, *Aureobasidium pullulans*, *Trichoderma* sp., *Chaetomium globosum* and *Rhizopus stolonifer* (data not shown).

In respect to the specific human immune responses to the *E. cuniculi* infection, anti-spore wall IgG was observed to precede anti-PT IgG (7). Strong antigenicity and immunogenicity of *E. cuniculi* PTP1 have also been reported (20). However, most of our subjects were negative for anti-spore wall IgM and IgG, as noted previously (10). Moreover, anti-PT IgG antibodies were not detectable in most of our subjects (10). Therefore, these subjects may have been exposed to *E. cuniculi* spores, but showed little secondary immune response to their exposure. There is still the possibility that such IgM antibodies are cross-reactive antibodies produced by fungal infections, since the primary response usually is of low specificity. In these regards, further work needs to be done.

Apart from some extremely rare situations, it is most unlikely that microsporidiosis is provoked by *E. cuniculi* in immunocompetent persons (2,4,8). Considering that almost all human encephalitozoonosis cases occurred in immunocompromised patients (2,4–6), one can speculate that protective immunity plays a very important role against *E. cuniculi* infection. We previously showed that the rate of positivity for anti-PT IgM antibodies was significantly higher among healthy people than among HIV-positive persons, such that the CD4 cell level greatly affected the detection of anti-PT IgM antibodies (10). It should be emphasized that human microsporidiosis is predominantly associated with $CD4^+$ T cell deficiency (8,22). A recent report on intraocular microsporidiosis in a patient with idiopathic $CD4^+$ T-lymphocytopenia proves the infectivity of *E. cuniculi* for immunodeficient humans (23).

In a model of PT discharge, it has been thought that unpolymerized PTP is released from the PT core and polymerizes on the outside of the membrane scaffolding as it is being everted (20). If circulating anti-PT IgM antibodies react with these unpolymerized and polymerized PTPs, resultant antigen–antibody complexes may block the formation of PTs, thus preventing the PT from penetrating a host cell. However, as in other human opportunistic protozoal infections, microsporidian-specific antibodies alone may not be protective (22). In humans, cell-mediated immunity is said to be critical for protection against microsporidian organisms (22). More recently, Sak *et al.* (24) demonstrated that humoral antibodies enhance the protective effect of $CD4^+$ T lymphocytes using SCID mice perorally infected with *E. cuniculi*, suggesting that the humoral part of the immune system may contribute to the defence against microsporidial infection. Further studies on human anti-PT IgM need to be performed from the perspective of protective immunity.

ACKNOWLEDGEMENTS

The authors appreciate the assistance of Shigeru Miwa (Immunobion, LTD., Sapporo, Japan) who contributed by producing the specific monoclonal antibody, MAb2. We also thank Tokiko Asakura for her assistance with the serological testing and cell culture.

This work was supported by Grant-in-Aid no. 16390177 from the Ministry of Education, Science, Sports and Culture of Japan.

REFERENCES

1 Canning EU & Varva J. Phylum Microsporidia. In Lee JJ, Leedale GF & Bradbury P (eds): *The Illustrated Guide to the Protozoa*, 2nd edn. Lawrence, KS, USA, Society of Protozoologists, 2000: 39–126.

2 Mathis A, Weber R & Deplazes P. Zoonotic potential of the Microsporidia. *Clin Microbiol Rev* 2005; **18**: 423–445.

3 Didier ES, Stovall ME, Green LC, Brindley PJ, Sestak K & Didier PJ. Epidemiology of microsporidiosis: sources and modes of transmission. *Vet Parasitol* 2004; **126**: 145–166.

4 Weber R, Schwartz DA & Deplazes P. Laboratory diagnosis of microsporidiosis. In Wittner M & Weiss LM (eds): *The Microsporidia and Microsporidiosis*. Washington, DC, ASM Press, 1999: 315–362.

5 Mohindra AR, Lee MW, Visvesvara G, *et al.* Disseminated microsporidiosis in a renal transplant recipient. *Transplant Infect Dis* 2002; **4**: 102–107.

6 Gamboa-Dominguez A, De Anda J, Donis J, Ruiz-Maza F, Visvesvara GS & Diliz H. Disseminated *Encephalitozoon cuniculi* infection in a Mexican kidney transplant recipient. *Transplantation* 2003; **75**: 1898–1900.

7 van Gool T, Biderre C, Delbac F, Wentink-Bonnema E, Peek R & Vivares CP. Serodiagnostic studies in an immunocompetent individual infected with *Encephalitozoon cuniculi*. *J Infect Dis* 2004; **189**: 2243–2249.

8 Bryan RT. Microsporidiosis as an AIDS-related opportunistic infection. *Clin Infect Dis* 1995; **21** (Suppl. 1): S62–S65.

9 Franzen C & Muller A. Microsporidiosis: human disease and diagnosis. *Microbes Infect* 2001; **3**: 389–400.

10 Omura M, Furuya K, Kudo S, Sugiura W & Azuma H. Detecting immunoglobulin M antibodies against microsporidian *Encephalitozoon cuniculi* polar tubes in sera from healthy and human immunodeficiency virus-infected persons in Japan. *Clin Vaccine Immunol* 2007; **14**: 168–172.

11 Asakura T, Nakamura S, Ohta M, Une Y & Furuya K. Genetically unique microsporidian *Encephalitozoon cuniculi* strain type III isolated from squirrel monkeys. *Parasitol Int* 2006; **55**: 159–162.

12 Galfre G, Howe SC, Milstein C, Butcher GW & Howard JC. Antibodies to major histocompatibility antigens produced by hybrid cell lines. *Nature* 1977; **266**: 550–552.

13 Duk M, Ugorski M & Lisowska E. β-elimination of *O*-glycans from glycoproteins transferred to immobilon P membranes: method and some applications. *Anal Biochem* 1997; **253**: 98–102.

14 Hellman U, Wernstedt C, Gonez J & Heldin CH. Improvement of an 'In-Gel' digestion procedure for the micropreparation of internal protein fragments for amino acid sequencing. *Anal Biochem* 1995; **224**: 451–455.

15 Xu Y & Weiss LM. The microsporidian polar tube: a highly specialized invasion organelle. *Int J Parasitol* 2005; **35**: 941–953.
16 Peuvel I, Peyret P, Metenier G, Vivares CP & Delbac F. The microsporidian polar tube: evidence for a third polar tube protein (PTP3) in *Encephalitozoon cuniculi*. *Mol Biochem Parasitol* 2002; **122**: 69–80.
17 Xu Y, Takvorian PM, Cali A, Orr G & Weiss LM. Glycosylation of the major polar tube protein of *Encephalitozoon hellem*, a microsporidian parasite that infects humans. *Infect Immun* 2004; **72**: 6341–6350.
18 van Gool T, Vetter JCM, Weinmayr B, Van Dam A, Derouin F & Dankert J. High seroprevalence of *Encephalitozoon* species in immunocompetent subjects. *J Infect Dis* 1997; **175**: 1020–1024.
19 Peek R, Delbac F, Speijer D, *et al.* Carbohydrate moieties of microsporidian polar tube proteins are targeted by immunoglobulin G in immunocompetent individuals. *Infect Immun* 2005; **73**: 7906–7913.
20 Keohane EM & Weiss LM. The structure, function, and composition of the microsporidian polar tube. In Wittner M & Weiss LM (eds): *The Microsporidia and Microsporidiosis*. Washington, DC, ASM Press, 1999: 196–224.
21 Thomarat F, Vivares CP & Gouy M. Phylogenetic analysis of the complete genome sequence of *Encephalitozoon cuniculi* supports the fungal origin of microsporidia and reveals a high frequency of fast-evolving genes. *J Mol Evol* 2004; **59**: 780–791.
22 Evering T & Weiss LM. The immunology of parasite infections in immunocompromised hosts. *Parasite Immunol* 2006; **28**: 549–565.
23 Kodjikian L, Garweg JG, Nguyen M, Schaffner T, Deplazes P & Zimmerli S. Intraocular microsporidiosis due to *Encephalitozoon cuniculi* in a patient with idiopathic CD4$^+$ T-lymphocytopenia. *Int J Med Microbiol* 2005; **294**: 529–533.
24 Sak B, Salat J, Horka H, Sakova K & Ditrich O. Antibodies enhance the protective effect of CD4$^+$ T lymphocytes in SCID mice perorally infected with *Encephalitozoon cuniculi*. *Parasite Immunol* 2006; **28**: 95–99.

Interleukin-4–Transgenic hu-PBL-SCID Mice: A Model for the Screening of Antiviral Drugs and Immunotherapeutic Agents against X4 HIV-1 Viruses

Kazu Okuma,[1] Reiko Tanaka,[1] Tomoyuki Ogura,[2] Mamoru Ito,[2] Sei Kumakura,[3] Mikiro Yanaka,[3] Masako Nishizawa,[4] Wataru Sugiura,[4] Naoki Yamamoto,[4] and Yuetsu Tanaka[1]

[1]Department of Immunology, Graduate School and Faculty of Medicine, University of the Ryukyus, Okinawa, [2]Central Institute for Experimental Animals, Kanagawa, and [3]Kureha Corporation and [4]National Institute of Infectious Diseases, Tokyo, Japan

CXCR4-tropic (X4) human immunodeficiency virus type 1 (HIV-1) does not efficiently infect and replicate in severe combined immunodeficiency (SCID) mice reconstituted with human peripheral blood mononuclear cells, termed "hu-PBL-SCID mice," due to, at least in part, relatively low levels of expression of the CXCR4 coreceptor. To overcome this limitation, interleukin (IL)–4–transgenic hu-PBL-SCID mice were derived that spontaneously synthesized human IL-4, which has been shown to enhance CXCR4 expression and promote X4 virus infection in vitro. Experiments reported here show that (1) synthesis of human IL-4 in vivo augmented CXCR4 expression on human CD4$^+$ lymphocytes and importantly led to productive infection of not only X4 HIV-1_{NL4-3} but also multidrug-resistant primary clinical isolates and that (2) the in vivo infection could be significantly blocked by the administration of a CXCR4 antagonist. Altogether, IL-4–transgenic hu-PBL-SCID mice provide a useful model for X4 HIV-1 study and testing/screening of anti-X4 viral drugs.

HIV-1 isolates enter target cells primarily after binding to the CD4 receptor and via the CXCR4 and CCR5 coreceptors [1–5] and are classified into X4 and R5 strains, respectively [6]. The X4 isolates are frequently implicated in the decline of peripheral CD4$^+$ T cell counts characteristic of the late stage of HIV-1 infection proceeding to the development of AIDS [7].

hu-PBL-SCID mice have been extensively used as a small animal model to study HIV-1 pathogenesis [8–14]. Results from a previous study showed that, although infection of human peripheral blood mononuclear cell (PBMC)–reconstituted hu-PBL-SCID mice with a predominantly R5 HIV-1 caused intensive CD4$^+$ T cell depletion, infection of similarly reconstituted mice with the same infectious dose of an X4 HIV-1 resulted in little or no CD4$^+$ T cell depletion [11]. Thereafter, it was noted that this limitation of X4 HIV-1 infection was due, at least in part, to a decrease in the intensity of CXCR4 expression on CD4$^+$ T cells [13]. Thus, it was reasoned that the pathogenic effects of the X4 HIV-1 strains in the hu-PBL-SCID mice might be related to the relative levels of the expression of HIV-1 coreceptor (the state of activation/differentiation) on human CD4$^+$ T cells at the time of infection in these mice. This limitation has to date restricted our ability to use this mouse model for understanding the mechanisms of X4 HIV-1 pathogenesis and for the evaluation of candidate therapeutics against X4 viruses. These findings prompted us to seek alternative strategies for the development of an improved hu-PBL-SCID mouse system that is permissive for infection/replication of X4 isolates.

Human interleukin (IL)–4 has been shown to specifically enhance the cell-surface expression of CXCR4 on

Received 1 May 2007; accepted 11 July 2007; electronically published 4 December 2007.

Potential conflicts of interest: none reported.

Presented in part: First International Workshop on Humanized Mice, Tokyo, 11–12 October 2006 (abstract P-15); 14th Conference on Retroviruses and Opportunistic Infections, Los Angeles, 25–28 February 2007 (abstract 496).

Financial support: Health and Labor Science Research Grant (Research on Publicly Essential Drugs and Medical Devices) from the Ministry of Health, Labor, and Welfare of Japan (grant H16-soyaku-004).

Reprints or correspondence: Dr. Kazu Okuma, Dept. of Immunology, Graduate School and Faculty of Medicine, University of the Ryukyus, Uehara 207, Nishihara-cho, Nakagami-gun, Okinawa 903-0215, Japan (kokuma@med.u-ryukyu.ac.jp).

The Journal of Infectious Diseases 2008; 197:134–41

0022-1899/2008/19701-0021$15.00
DOI: 10.1086/524303

resting peripheral blood T cells [15]. Furthermore, it has been reported that human IL-4 plays an important role in rendering $CD4^+$ T cells susceptible to X4 HIV-1 infection via enhanced cell-surface expression of the CXCR4 coreceptor in vitro [15–17].

In efforts to overcome the limitation inherent with the use of hu-PBL-SCID mice for the study of X4 HIV-1 as described above, we developed an IL-4–transgenic immunodeficient mouse model that consistently secreted readily detectable serum levels of human IL-4. We show here that X4 isolates readily infect/replicate in this mouse model but not in wild-type (wt) non–IL-4–transgenic mice and that this model can now be exploited for the rapid evaluation of the therapeutic efficacy of new anti-X4 HIV-1 agents in vivo.

METHODS

IL-4–producing mice. Two strains of human IL-4–transgenic immunodeficient mice were bred on the C.B-17-*scid* [18] and BALB/cA-Rag2$^{-/-}\gamma_c^{-/-}$ (dKO) genetic background mice [19, 20] at the Central Institute for Experimental Animals (CIEA) as follows. PBMCs were isolated from a healthy human volunteer and activated in vitro with pokeweed mitogen. RNA was prepared from these PBMCs, and then cDNA was synthesized by reverse-transcriptase polymerase chain reaction (PCR). Human IL-4 cDNA was amplified from the cDNA using one set of primers: 5'-CCCGGGATCGTTAGCTTCTCCTGATAAAA-3' and 5'-GCGGCCGCTATTCAGCTCGAACACTTTGAAT-3'. The product was inserted into the PCR2.1 vector by use of the TA cloning kit (Invitrogen) and the insert sequenced. After confirmation of the sequence, IL-4 cDNA was inserted into pCMVb with a CMV promoter (Invitrogen). To produce transgenic mice, a DNA fragment containing the CMV promoter, IL-4 cDNA, and Poly(A) regions was excised with *Xho*I and *Hind*III sites of pCMVb and microinjected into the pronuclei of fertilized eggs from the 2 strains (C.B-17-*scid* and BALB/cA-dKO) of mice. These eggs were subsequently transplanted into oviducts of pseudopregnant foster recipient mice. The offspring mice were screened to confirm the insertion of the transgene into the genome by PCR, and serum from these mice was screened for levels of human IL-4 by ELISA with a commercial kit (BD). The IL-4 transgene–hemizygous mice were maintained by mating them with wt mice with the same genetic background in the specific-pathogen–free (SPF) facility of the CIEA. The mice were transferred to the SPF and biosafety level 3 facilities of the Institute for Animal Experiments, University of the Ryukyus, and were used for further experiments. The experimental protocols were approved by the Institutional Animal Care and Use Committee on the basis of the Regulation for Animal Experimentation of the CIEA and University of the Ryukyus before the initiation of the study.

Viruses. X4 HIV-1_{NL4-3} was obtained as described elsewhere [14]. Fourteen multidrug-resistant (MDR) HIV-1 clinical isolates were obtained from HIV-1–infected patients who had been treated with highly active antiretroviral therapy (HAART). The viruses were propagated in PBMCs stimulated with phytohemagglutinin (PHA; Sigma), IL-2 (National Institutes of Health AIDS Research and Reference Reagent Program), and IL-4 (Peprotec). Three isolates from these MDR isolates that efficiently grew in the activated cells were selected for further experiments. The titers of virus stocks were determined by end-point titration using a 2-fold limiting dilution of the stock and in vitro PHA-activated human PBMCs, and the infectious units (IU) were calculated.

CXCR4 antagonist. The synthesis and purification of the CXCR4 antagonist KRH-1636 were performed at Kureha Corporation as described elsewhere [21]. As a control, the carrier tartrate was used in parallel.

Transplantation and infection. The control (wt) and the IL-4–transgenic C.B-17-*scid* mice were depleted of NK cells by the intraperitoneal (ip) injection of 0.5–1.0 mg of anti–mouse IL-2Rβ (TMβ-1) [22] per animal. The IL-4–transgenic and the control BALB/cA-dKO mice do not require TMβ-1 treatment because they lack NK cells [19, 20]. PBMCs were isolated from healthy human donors. Groups of 2–4-month-old IL-4–transgenic mice from each of the 2 background strains and their corresponding non–IL-4–transgenic wt mice were injected ip with PBMCs 3 days later. Groups of mice were challenged 24 h later ip with mock, HIV-1_{NL4-3}, or MDR isolates (2000 IU/500 μL/animal). For the experiments using the CXCR4 antagonist, groups of mice were administered 0.1 mL of 10 mmol/L KRH-1636, the tartrate carrier or saline ip at 1 h before and 1 day after virus infection. At 6–8 days after infection, the mice were killed, their blood was obtained by cardiocentesis, and human lymphocytes were collected from the peritoneal lavage fluids. The serum samples were assayed for levels of human IL-4 by use of an ELISA kit (R&D Systems). The human lymphocytes were analyzed using flow cytometry as described below. The remaining cells were cultured in RPMI 1640 medium (Sigma) supplemented with fetal calf serum and IL-2. The peritoneal lavage fluids, serum samples, and lymphocyte culture supernatants were examined for levels of p24 by use of an ELISA kit (Zepto Metrix).

Flow cytometry analysis. Cell samples to be analyzed by flow cytometry were initially incubated with normal human IgG for blocking of the Fc receptors. For cell-surface staining, aliquots of cells were then stained with Cy5-labeled anti-CD4 (OKT4) and phycoerythrin-labeled anti-CXCR4 (12G5; Dako) or with Cy5-labeled anti-CD3 (OKT3). For intracellular staining, after CD3 staining the aliquots of cells were fixed, permeabilized, and incubated with fluorescein isothiocyanate–labeled anti–HIV-1 Gag p24 (2C2; Y.T. et al., unpublished data). Stained samples were analyzed on a FACSCalibur flow cytometer, using Cell Quest software (BD Pharmingen). Aliquots of cells stained

Table 1. Expression of human CD4, CXCR4, and intracellular HIV-1 p24 in cells from X4 HIV-1–infected hu-PBL-SCID mice.

Category	X4 HIV-1 infection	Mice, no.	$CD4^+$ T cells, %	*P*	$CXCR4^+CD4^+$ T cells, %	*P*	$p24^+$ T cells, %	*P*
C.B-17-*scid* mice								
Control	NL4-3	6	22.1 ± 8.3	<.001	45.2 ± 4.7	<.001	0.1 ± 0.1	NS
IL-4 transgenic	NL4-3	6	66.3 ± 9.0		85.5 ± 5.1		0.1 ± 0.1	
BALB/cA-dKO mice								
Control	NL4-3	5	35.9 ± 5.1	<.01	32.6 ± 1.4	<.001	0.2 ± 0.1	<.05
IL-4 transgenic	NL4-3	3	57.4 ± 8.3		68.2 ± 3.9		3.2 ± 1.2	

NOTE. Cells in peritoneal lavage fluid from control and interleukin (IL)–4–transgenic hu-PBL-SCID mice on either the C.B-17-*scid* or BALB/cA-dKO background were labeled with appropriate monoclonal antibodies and analyzed by flow cytometry, as described in Methods. Analyzed data are shown as mean ± SD values. NS, not significant. The indicated *P* values for the comparison of control vs. transgenic mice for each category are based on Student's *t* test.

with or without each of the antibodies described above were used as controls for the purposes of establishing gates and for the determination of the frequency of positive cells.

Statistical analysis. Data obtained by flow cytometry were analyzed by Student's *t* test with GraphPad Prism (version 4.0c for Mac OS X; GraphPad Software).

RESULTS

Production of human IL-4 in IL-4–transgenic mice. Efforts to construct the IL-4–transgenic mice constitutively synthesizing human IL-4 finally led to the establishment of mice on each of the 2 immunodeficient backgrounds expressing either high or low serum levels of human IL-4 (data not shown). On the basis of preliminary data obtained on the efficiency of virus replication, all subsequent experiments were done using only the 2 strains with high serum IL-4 expression levels. We assayed for levels of human IL-4 in the serum from the $IL\text{-}4^+$ hu-PBL-SCID mice and the wt hu-PBL-SCID mice on either the C.B-17-*scid* or BALB/cA-dKO background after infection with X4 HIV-$1_{NL4\text{-}3}$. Serum from each of the IL-4–transgenic mice on either background contained significant levels of human IL-4 (~800–1800 pg/mL), whereas serum from the control mice on the same background showed nondetectable levels of human IL-4. These data demonstrate that the human IL-4 synthesized by the IL-4–transgenic mice is generated from the transgene but not from the human PBMCs transplanted in these mice.

Effect of human IL-4 on the levels of human CXCR4 and CD4 expression by cells transplanted into mice. Since human IL-4 has been previously documented to enhance the expression of CXCR4 in vitro, experiments were done to examine the expression of human CXCR4 on transplanted $CD4^+$ cells in the peritoneal lavage fluids from HIV-$1_{NL4\text{-}3}$–infected $IL\text{-}4^+$ hu-PBL-SCID mice and control hu-PBL-SCID mice on either the C.B-17-*scid* or BALB/cA-dKO background. There did not appear to be any detectable difference in the absolute amounts of cells recovered from the peritoneal lavage fluids from the IL-4–positive or IL-4–negative hu-PBL-SCID mice on either background (data not shown). Flow cytometry analysis demonstrated that the frequency of human $CD4^+$ cells from the IL-4–transgenic C.B-17-*scid* or BALB/cA-dKO mice was significantly higher than that from the control mice (table 1). As expected, there was a marked increase in the frequency of CXCR4-expressing $CD4^+$ cells from the IL-4–transgenic mice on either genetic background relative to that from the control mice (figure 1*A* and table 1). Thus, these data indicate that human IL-4 produced endogenously is functional in vivo in terms of its ability to enhance human CXCR4 expression on $CD4^+$ cells transplanted into the mice.

Increased frequency of X4 HIV-1–infected cells from IL-4–transgenic hu-PBL-SCID mice. Since the constitutive synthesis of human IL-4 in IL-4–transgenic hu-PBL-SCID mice resulted in the enhanced expression of X4 HIV-1 receptors (human CXCR4/CD4) on the transplanted cells, we reasoned that such cells were likely to be more permissive to the infection and replication of X4 HIV-1. We thus challenged the IL-4–transgenic hu-PBL-SCID mice and control hu-PBL-SCID mice bred on the C.B-17-*scid* or BALB/cA-dKO mice with HIV-$1_{NL4\text{-}3}$. Cells obtained from the peritoneal lavage fluids were analyzed for cell-surface expression of human CD3 (since HIV-1 downmodulates CD4 expression) and the presence of intracellular p24. As seen in figure 1*B* and table 1, although very few if any $CD3^+$ cells from the control or IL-4–transgenic C.B-17-*scid* mice showed p24 expression, there was a >10-fold increase in the frequency of $CD3^+$ T cells that expressed p24 from the IL-4–transgenic BALB/cA-dKO mice relative to the control mice. These data suggest that, while transgene-induced human IL-4 increases the frequency of $CD4^+CXCR4^+$ T cells transplanted into both the C.B-17-*scid* and the BALB/cA-dKO mice, only the latter demonstrates increased sensitivity to X4 HIV-1 infection and replication, at least when this assay is used (see below).

High production of X4 HIV-1 in the culture supernatants of cells from IL-4–transgenic hu-PBL-SCID mice. In an effort

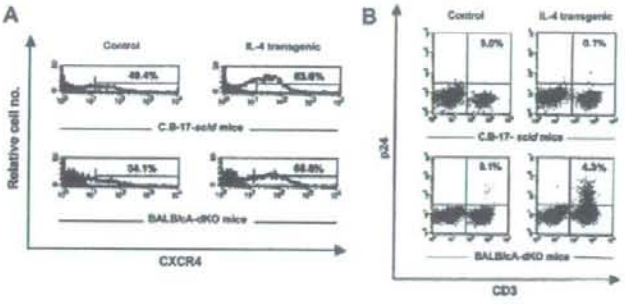

Figure 1. Enhancement of the expression of CXCR4 coreceptor and facilitation of X4 HIV-1 infection and replication in hu-PBL-SCID mice by in vivo production of human interleukin (IL)–4. Groups of hu-PBL-SCID mice, generated from IL-4–transgenic and nontransgenic (control) mice on either the C.B-17-*scid* or BALB/cA-dKO background, were injected intraperitoneally with HIV-1_{NL4-3} at −24 h after peripheral blood mononuclear cell (PBMC) reconstitution. Six to eight days later, peritoneal lavage fluids were harvested from mice in each group, and cells were collected from the fluids by density-gradient centrifugation. *A*, Cells analyzed for the frequency and mean density of human CXCR4 expression on CD4$^+$ cells by flow cytometry. Data for analyzed cells are depicted by a thick line, and the background control profile is depicted by a thin line and gray shading. The nos. above the bars represent the percentage of positive cells. Data shown are representative of mice in each group from 3 independent experiments. *B*, HIV-1 infectivity. Cells were subjected to flow cytometry after cell-surface CD3 and intracellular p24 staining. Analyzed data are depicted as dot plots. The nos. in the graphs indicate the percentage of CD3$^+$p24$^+$ cells. Data displayed are representative of mice in each group from 3 independent experiments.

to determine the reason for our failure to detect levels of intracellular p24 in the IL-4–transgenic mice on the C.B-17-*scid* background and to further support the above finding, peritoneal lavage fluids were collected from mock- or HIV-1_{NL4-3}–infected IL-4$^+$ hu-PBL-SCID mice and, for purposes of control, the HIV-1_{NL4-3}–infected non–IL-4–transgenic mice on the C.B-17-*scid* background. The cells were isolated from the peritoneal lavage fluids, and an aliquot was analyzed for the frequency and the relative density of human CXCR4/CD4; the remaining aliquot was cultured in vitro. In addition, the peritoneal lavage fluids and the culture supernatants of cells at days 1–3 after culture were assayed for levels of p24 production. As displayed in table 2, although the frequency of CXCR4$^+$CD4$^+$ cells in the IL-4–transgenic mice was significantly higher than that in the nontransgenic mice, the mean fluorescence intensity (MFI) of CXCR4 expressed by the CD4$^+$ T cells from these mice was not increased compared with the control (because of an increase in the frequency of CXCR4$^+$CD4$^+$ cells with relatively low MFI; see figure 1*A*). Analysis of levels of synthesized p24 demonstrated marked differences, as shown in figure 2. Thus, although the amounts of p24 produced were modest in the peritoneal lavage fluids and the cell-culture supernatants from HIV-1–infected control mice, the levels of p24 produced by those from HIV-1–infected IL-4–transgenic mice were strikingly higher (15,429, 11,844, 1696, and 53 pg/mL in the supernatants on day 3) (mean, 48.9 vs. 7255 pg/mL; >100-fold increase). Although the levels of p24 produced by one of the IL-4–transgenic mice (mouse 12) were similar to those in the control mice, this was likely due to the much lower relative level of human IL-4 (354 pg/mL in serum) produced by mouse 12 than those from the other 3 IL-4–transgenic mice (4227, 6313, and 2356 pg/mL in serum). The present data not only document the fact that the cells from these

Table 2. Effect of the CXCR4 antagonist KRH-1636 on the expression of human CXCR4 by CD4$^+$ cells from X4 HIV-1–infected interleukin (IL)–4–transgenic hu-PBL-SCID mice.

C.B-17-*scid* mice	X4 HIV-1 Infection	CXCR4 antagonist	Mice, no.	CXCR4$^+$CD4$^+$ T cells, %	*P*	CXCR4 on CD4$^+$ T cells, MFI	*P*
Control	NL4-3	Mock	4	45.5 ± 9.3	<.05[a]	73.7 ± 36.0	NS[a]
IL-4 transgenic	NL4-3	Mock	4	66.7 ± 7.4	NS[b]	73.1 ± 6.2	<.05[b]
IL-4 transgenic	NL4-3	KRH-1636	4	63.0 ± 4.2		62.2 ± 4.8	

NOTE. Control or IL-4–transgenic hu-PBL-SCID mice on the C.B-17-*scid* background infected with X4 HIV-1_{NL4-3} were administered mock KRH-1636 or real KRH-1636. Cells isolated from the peritoneal lavage fluid from the mice in each group were labeled with appropriate monoclonal antibodies and subjected to flow cytometry, as described in Methods. Data analyzed are displayed as mean ± SD values. MFI, mean fluorescence intensity; NS, not significant. The indicated *P* values are based on Student's *t* test.

[a] For the comparison between control mice and IL-4–transgenic mice that received a mock CXCR4 antagonist.

[b] For the comparison between IL-4–transgenic mice that received a mock CXCR4 antagonist and IL-4–transgenic mice that received KRH-1636.

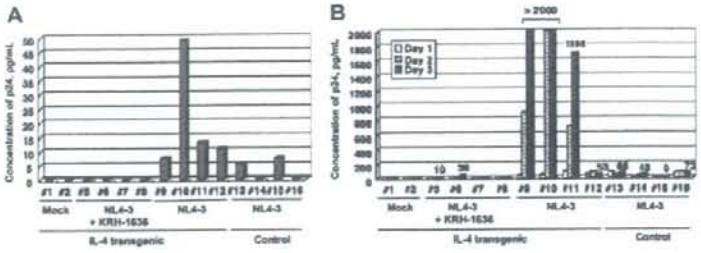

Figure 2. Efficient infection of interleukin (IL)–4–producing hu-PBL-SCID mice with X4 laboratory strain and an inhibitory effect of the CXCR4 antagonist KRH-1636 on infection. Twelve IL-4–transgenic and 4 nontransgenic (control) hu-PBL-SCID mice were generated on the C.B-17-*scid* background. Among them, 8 IL-4–transgenic and 4 control mice were infected intraperitoneally (ip) with the X4 laboratory strain (HIV-1_{NL4-3}) and 4 IL-4–transgenic mice were mock-infected at 1 day after engraftment. To evaluate the effect of KRH-1636, this drug was administered ip twice, at 1 h before and 1 day after infection of 4 IL-4–transgenic mice (NL4-3 + KRH-1636). At 8 days after infection, peritoneal lavage fluids were obtained from the mice in each group. Cells were isolated from the fluids and cultured in IL-2–containing medium. Levels of HIV-1 p24 in the peritoneal lavage fluids *(A)* and culture supernatants at days 1–3 after incubation *(B)* were quantitated for infectivity and replication efficiency by ELISA. With regard to the data on mock-infected mice, only 2 of 4 representative data are presented. The nos. listed above the bars in the graph indicate levels of HIV-1 p24 when it was detectable on day 3 (most of the values were <200 pg/mL, and select samples showed values of >2000 pg/mL). Pound signs (#) indicate mouse nos. Results shown are representative of 3 independent experiments.

IL-4–transgenic C.B-17-*scid* mice are susceptible but also demonstrate that the virus from such cells is replication competent. In addition, these findings suggest that the use of intracellular p24 levels is not a sensitive enough technique and that data using the intracellular p24 assay need to be carefully evaluated. These data also indicate that the IL-4–transgenic hu-PBL-SCID mice provide a powerful model for the study of X4 HIV-1 infection independently of the genetic background of the mice.

Inhibitory effect of the CXCR4 antagonist on infection of IL-4–transgenic hu-PBL-SCID mice with the X4 laboratory strain. In an effort to further validate that the CXCR4 coreceptor was indeed used by the X4 HIV-1 virus in the IL-4–transgenic hu-PBL-SCID mice, we used the X4 virus-entry inhibitor, CXCR4 antagonist KRH-1636. Thus, the IL-4–transgenic hu-PBL-SCID mice on the C.B-17-*scid* background were infected with X4 laboratory strain HIV-1_{NL4-3} and were either mock treated or treated with KRH-1636, and the peritoneal lavage fluids, cells in fluids, and cell-culture supernatants were examined as described above. As shown in table 2, the frequency of $CXCR4^+CD4^+$ cells in KRH-1636–treated IL-4–transgenic mice was marginally lower than that in mock-treated IL-4–transgenic mice. In addition, the MFI of CXCR4 expression by the $CD4^+$ T cells was clearly reduced by KRH-1636 administration. Importantly, treatment with KRH-1636 almost completely blocked X4 HIV-1 infection in these IL-4–transgenic mice (figure 2). These data indicate that X4 HIV-1 infection in transgenic mice is CXCR4 dependent and that our mouse model can be used to develop and test new anti-X4 HIV-1 drugs in vivo.

Therapeutic effect of KRH-1636 on the infection of IL-4–transgenic hu-PBL-SCID mice with MDR clinical isolates. The appearance of MDR HIV-1 clinical isolates has been and continues to be one of the growing problems in a significant number of patients receiving HAART and seriously limits the use of the antiviral drugs that are currently available. Thus, the development of novel adjunct or alternative therapeutics is an urgent need. Since treated patients tend to harbor significantly higher levels of either dual/mixed or X4 viruses [23] and since MDR isolates are not usually refractory to new treatment with drugs from classes that have not been used previously in patients from which the viruses were derived, we finally wanted to examine the effect of KRH-1636 on MDR HIV-1 infection in IL-4–transgenic hu-PBL-SCID mice. For this experiment, we used the IL-4–transgenic BALB/cA-dKO mice instead of the IL-4–transgenic C.B-17-*scid* mice, because the former seems more permissive to X4 HIV-1 infection than the latter, as described above. Before the in vivo study, we confirmed that the in vitro infection by 3 MDR clinical isolates could be inhibited with KRH-1636 (more than ~90% inhibition at the 5-μmol/L level). Thus, groups of IL-4–transgenic hu-PBL-SCID mice were infected with a mixture of these selected MDR isolates containing equal IU of each virus and treated with KRH-1636 or the tartrate carrier control. Thereafter, the cells obtained from the peritoneal lavage fluids were analyzed for the expression of cell-surface human CD4, CD3, and intracellular p24. The serum, peritoneal lavage fluids, and supernatants following in vitro culture of the cells for 24 h were assayed for levels of p24 production. Flow cytometry analysis after CD4 staining demonstrated a significant decline in $CD4^+$ T cells in 2 (mouse 7 and mouse 8) of 4 control-treated mice (figure 3*A*; top profile shows data from 1 of these 2 mice), which was likely due to MDR HIV-1 pathogenesis. However, importantly, no detectable depletion of $CD4^+$ T cells was observed in any of 4 KRH-1636–treated mice (figure 3*A*; bottom profile). As summarized in table 3, the difference in the frequency of $CD4^+$ T cells between the control-treated mice and the

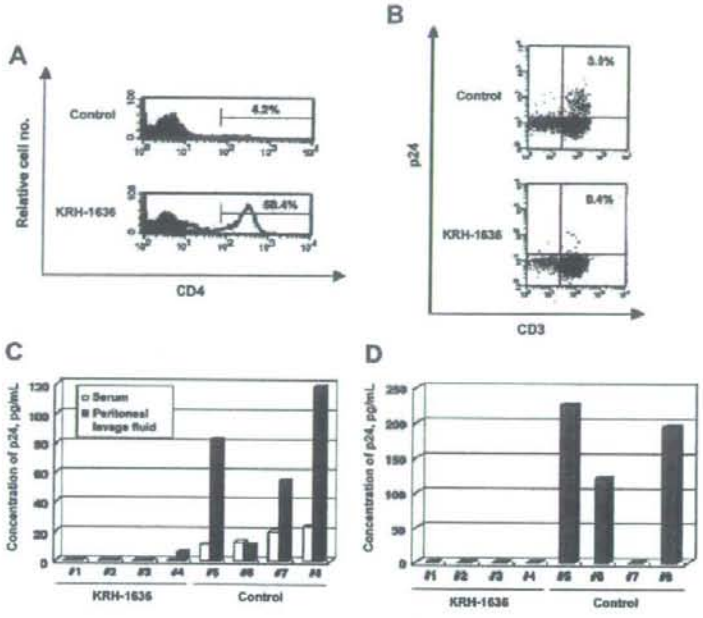

Figure 3. Prophylactic effect of KRH-1636 on infection and pathogenesis by multidrug-resistant (MDR) HIV-1 clinical isolates. Eight interleukin (IL)–4–transgenic hu-PBL-SCID mice (BALB/cA-dKO) were infected intraperitoneally (ip) with a mixture of MDR HIV-1 clinical isolates at 1 day after human peripheral blood mononuclear cell transfer. In an effort to assess the effect of KRH-1636 on HIV-1 infection, this agent or tartrate (control drug) was administered to 4 mice per group ip twice, at 1 h before infection and 1 day after infection. At 7 days after infection, serum and peritoneal lavage fluids were harvested from mice in each group, and cells were collected from the fluids. *A*, Cells examined for human CD4 expression by cell-surface staining and standard flow cytometry. Representative data from a single mouse from the control-treated or the KRH-1636–treated HIV-1–infected mice are shown. The frequency of $CD4^+$ T cells is depicted by a thick line, and the background control is depicted by a thin line with gray shading. The nos. above the bars indicate the percentage of positive cells. *B*, Aliquot of the peritoneal lavage cells analyzed by flow cytometry for the frequency of $CD3^+$ T cells that were positive for the intracellular presence of HIV-1 p24. Representative data of cells from the control-treated and the KRH-1636–treated HIV-1–infected mice are shown. The nos. in the graphs indicate the percentage of $CD3^+p24^+$ cells. *C*, Concentrations of p24 in serum and peritoneal lavage fluid. Concentrations were determined by ELISA to quantify MDR HIV-1 infection and replication efficiency. Pound signs (#) indicate mouse nos. *D*, Levels of in vitro p24 production. The remaining cells were cultured in a microtiter plate containing $IL\text{-}2^+$ medium for ~24 h, and the culture supernatants obtained were assayed for levels of in vitro p24 production by ELISA. Pound signs (#) indicate mouse nos. Results shown are representative of 3 similar independent experiments.

KRH-1636–treated mice was not significant. However, the MFI of CD4 expression was significantly decreased in the control-treated mice (229.3 vs. 296.3; $P < .05$). Results of CD3/p24 staining showed that the frequency of $CD3^+p24^+$ cells was markedly inhibited in the KRH-1636–treated mice, compared with that in the carrier-treated control mice (figure 3*B* and table 3). Furthermore, levels of HIV-1 p24 in the serum samples, peritoneal lavage fluids, and culture supernatants from the KRH-

Table 3. Effect of KRH-1636 on infection and pathogenesis by multidrug-resistant (MDR) HIV-1 clinical isolates in interleukin (IL)–4–transgenic hu-PBL-SCID mice.

BALB/cA-dKO mice	X4 HIV-1 infection	CXCR4 antagonist	Mice, no.	$CD4^+$ T cells, %	*P*	$CD4^+$ T cells, MFI	*P*	$p24^+$ T cells, %	*P*
IL-4 transgenic	MDR	Control	4	14.7 ± 11.9	NS	229.3 ± 33.0	<.05	3.2 ± 0.8	<.01
IL-4 transgenic	MDR	KRH-1636	4	31.3 ± 15.7		296.3 ± 25.2		0.8 ± 0.7	

NOTE. IL-4–transgenic hu-PBL-SCID mice on the BALB/cA-dKO background were infected with MDR HIV-1 clinical isolates and administered tartrate (control) or KRH-1636. Cells in peritoneal lavage fluid from the mice in each group were stained with appropriate monoclonal antibodies and analyzed by flow cytometry, as described in Methods. Data shown here are mean ± SD values. MFI, mean fluorescence intensity; NS, not significant. The indicated *P* values for the comparison between control mice and mice that received KRH-1636 are based on Student's *t* test.

1636–treated HIV-1–infected mice were almost completely reduced relative to those in the control mice (figure *3C* and *3D*). Note that the failure to detect the in vitro production of p24 in mouse 7 might result from depletion of $CD4^+$ T cells (figure *3D*). These data demonstrate that the CXCR4 antagonist KRH-1636 has a marked degree of prophylactic effect on infection with pathogenic MDR clinical isolates in vivo.

DISCUSSION

Humanized mice that have served as valuable small animal models include the SCID-hu Thy/Liv mouse [24–28]. This mouse model, generated by implanting human hematopoietic tissues (human fetal thymus/liver) under the kidney capsule, has been used for the study of HIV-1 and is known for permissiveness to X4 HIV-1 infection [26–28]. However, the use of this model is limited by the fact that the implants are of human fetal organ origins that are not easily available. On the other hand, the hu-PBL-SCID mouse model provides another surrogate in vivo HIV-1 infection assay system. Although this model has led to a number of successful studies of HIV-1 [8–14], there was still a limitation in that it was difficult to demonstrate X4 HIV-1 infection and replication in such mice. Thus, to add extra value to the use of this mouse system for the study of HIV-1, in the present study we developed novel human IL-4–transgenic hu-PBL-SCID mice that enable CXCR4-using HIV-1 strains to efficiently infect and replicate in these mice.

Human IL-4 has low homology with murine IL-4 both at the gene and protein levels, accounting for the lack of cross-reactivity of this cytokine in the 2 species in vitro [29–32]. Results of the experiments reported here indicate that the high efficiency of X4 HIV-1 infection in the IL-4–transgenic hu-PBL-SCID mice was, at least in part, secondary to enhanced expression of viral receptors induced by human IL-4 synthesized endogenously. Interestingly, although there was no apparent increase in the number of cells recovered from the engrafted transgenic mice, there was a significant increase in the number of $CD4^+$ T cells recovered (1.5–3-fold). It is thus possible that the other cell lineages migrate from the peritoneal cavity to other tissues of the mice, resulting in enrichment of the $CD4^+$ T cell lineage. However, further studies of other tissues are needed to clarify this issue. Furthermore, our preliminary experiments indicate that the IL-4–transgenic hu-PBL-SCID mice remain permissive to R5 strain infection (data not shown).

In this report, we created 2 types of novel hu-PBL-SCID mice by transplanting human PBMCs into IL-4–transgenic C.B-17-*scid* and BALB/cA-dKO mice. The data obtained show that hu-PBL-SCID mice using the IL-4–producing BALB/cA-dKO mice appeared more permissive to X4 HIV-1 infection than did those using the IL-4–producing C.B-17-*scid* mice, at least as determined by the presence of intracellular p24. Although the reasons for this difference remain to be determined, it should be noted that, whereas the BALB/cA-dKO mice were derived by double mutation with defects in both the recombinase-activating gene 2 (Rag-2) and the gene encoding the γ_c chain of select cytokine receptors [19, 20], the C.B-17-*scid* mice have only the Rag-2 mutation [18]. Thus, although the Rag-2 mutation prevents the normal maturation of T and B lymphocytes, the γ_c chain mutation abrogates the expression of functional receptors for IL-2 and other cytokines, preventing the expansion of lymphocytes, including NK cells, which play an important role in the innate immune response such as nonspecific rejection of xenogeneic grafts. It is thus possible that the C.B-17-*scid* mice maintain a low but significant residual level of NK cell function, which may play a role in the difference noted above even though they were administered significant levels of anti–IL-2Rβ antibody. Since the BALB/cA-dKO mice are completely deficient in NK cell lineage and function, they are more immunodeficient than the C.B-17-*scid* mice, suggesting that the level and type of immunodeficiency in the BALB/cA-dKO mice may facilitate better engraftment and more efficient viral infection and propagation within these mice. These select defects of the BALB/cA-dKO mice might render the IL-4–transgenic mouse model on this background more valuable and ideal for studies of X4 HIV-1.

Acknowledgments

We thank the National Institutes of Health AIDS Research and Reference Reagent Program and M. Sasaki for supplying interleukin-2 and technical support, respectively. We are also grateful to Prof. Aftab Ansari for his critical reading of the manuscript and for his helpful discussion about and suggestions for the manuscript.

References

1. Feng Y, Broder CC, Kennedy PE, Berger EA. HIV-1 entry cofactor: functional cDNA cloning of a seven-transmembrane, G protein-coupled receptor. Science **1996**; 272:872–7.
2. Alkhatib G, Combadiere C, Broder CC, et al. CC CKR5: a RANTES, MIP-1alpha, MIP-1beta receptor as a fusion cofactor for macrophage-tropic HIV-1. Science **1996**; 272:1955–8.
3. Berson JF, Long D, Doranz BJ, Rucker J, Jirik FR, Doms RW. A seven-transmembrane domain receptor involved in fusion and entry of T-cell-tropic human immunodeficiency virus type 1 strains. J Virol **1996**; 70: 6288–95.
4. Deng H, Liu R, Ellmeier W, et al. Identification of a major co-receptor for primary isolates of HIV-1. Nature **1996**; 381:661–6.
5. Doranz BJ, Rucker J, Yi Y, et al. A dual-tropic primary HIV-1 isolate that uses fusin and the beta-chemokine receptors CKR-5, CKR-3, and CKR-2b as fusion cofactors. Cell **1996**; 85:1149–58.
6. Berger EA, Doms RW, Fenyo EM, et al. A new classification for HIV-1. Nature **1998**; 391:240.
7. Xiao L, Rudolph DL, Owen SM, Spira TJ, Lal RB. Adaptation to promiscuous usage of CC and CXC-chemokine coreceptors in vivo correlates with HIV-1 disease progression. AIDS **1998**; 12:F137–43.
8. Mosier DE. Adoptive transfer of human lymphoid cells to severely immunodeficient mice: models for normal human immune function, autoimmunity, lymphomagenesis, and AIDS. Adv Immunol **1991**; 50:303–25.
9. Mosier DE, Gulizia RI, Baird SM, Wilson DB, Spector DH, Spector SA. Human immunodeficiency virus infection of human-PBL-SCID mice. Science **1991**; 251:791–4.

10. Torbett BE, Picchio G, Mosier DE. hu-PBL-SCID mice: a model for human immune function, AIDS, and lymphomagenesis. Immunol Rev **1991**; 124:139–64.
11. Mosier DE, Gulizia RJ, MacIsaac PD, Torbett BE, Levy JA. Rapid loss of CD4+ T cells in human-PBL-SCID mice by noncytopathic HIV isolates. Science **1993**; 260:689–92.
12. Rizza P, Santini SM, Logozzi MA, et al. T-cell dysfunctions in hu-PBL-SCID mice infected with human immunodeficiency virus (HIV) shortly after reconstitution: in vivo effects of HIV on highly activated human immune cells. J Virol **1996**; 70:7958–64.
13. Fais S, Lapenta C, Santini SM, et al. Human immunodeficiency virus type 1 strains R5 and X4 induce different pathogenic effects in hu-PBL-SCID mice, depending on the state of activation/differentiation of human target cells at the time of primary infection. J Virol **1999**; 73:6453–9.
14. Yoshida A, Tanaka R, Murakami T, et al. Induction of protective immune responses against R5 human immunodeficiency virus type 1 (HIV-1) infection in hu-PBL-SCID mice by intrasplenic immunization with HIV-1-pulsed dendritic cells: possible involvement of a novel factor of human $CD4^+$ T-cell origin. J Virol **2003**; 77:8719–28.
15. Jourdan P, Abbal C, Noraz N, et al. IL-4 induces functional cell-surface expression of CXCR4 on human T cells. J Immunol **1998**; 160:4153–7.
16. Tanaka Y, Koyanagi Y, Tanaka R, Kumazawa Y, Nishimura T, Yamamoto N. Productive and lytic infection of human CD4+ type 1 helper T cells with macrophage-tropic human immunodeficiency virus type 1. J Virol **1997**; 71:465–70.
17. Suzuki Y, Koyanagi Y, Tanaka Y, et al. Determinant in human immunodeficiency virus type 1 for efficient replication under cytokine-induced $CD4^+$ T-helper 1 (Th1)- and Th2-type conditions. J Virol **1999**; 73:316–24.
18. Bosma GC, Custer RP, Bosma MJ. A severe combined immunodeficiency mutation in the mouse. Nature **1983**; 301:527–30.
19. Traggiai E, Chicha L, Mazzucchelli L, et al. Development of a human adaptive immune system in cord blood cell-transplanted mice. Science **2004**; 304:104–7.
20. Berges BK, Wheat WH, Palmer BE, Connick E, Akkina R. HIV-1 infection and CD4 T cell depletion in the humanized $Rag2^{-/-}\gamma c^{-/-}$ (RAG-hu) mouse model. Retrovirology **2006**; 3:76.
21. Ichiyama K, Yokoyama-Kumakura S, Tanaka Y, et al. A duodenally absorbable CXC chemokine receptor 4 antagonist, KRH-1636, exhibits a potent and selective anti-HIV-1 activity. Proc Natl Acad Sci USA **2003**; 100:4185–90.
22. Tanaka T, Kitamura F, Nagasaka Y, Kuida K, Suwa H, Miyasaka M. Selective long-term elimination of natural killer cells in vivo by an anti-interleukin 2 receptor beta chain monoclonal antibody in mice. J Exp Med **1993**; 178:1103–7.
23. Hunt PW, Harrigan PR, Huang W, et al. Prevalence of CXCR4 tropism among antiretroviral-treated HIV-1–infected patients with detectable viremia. J Infect Dis **2006**; 194:926–30.
24. Goldstein H, Pettoello-Mantovani M, Katopodis NF, Kim A, Yurasov S, Kollmann TR. SCID-hu mice: a model for studying disseminated HIV infection. Semin Immunol **1996**; 8:223–31.
25. McCune JM. Animal models of HIV-1 disease. Science **1997**; 278:2141–2.
26. Aldrovandi GM, Feuer G, Gao L, et al. The SCID-hu mouse as a model for HIV-1 infection. Nature **1993**; 363:732–6.
27. Bierkowitz RD, Alexander S, Bare C, et al. CCR5- and CXCR4-utilizing strains of human immunodeficiency virus type 1 exhibit differential tropism and pathogenesis in vivo. J Virol **1998**; 72:10108–17.
28. Bonyhadi ML, Rabin L, Salimi S, et al. HIV induces thymus depletion in vivo. Nature **1993**; 363:728–32.
29. Yokota T, Otsuka T, Mosmann T, et al. Isolation and characterization of a human interleukin cDNA clone, homologous to mouse B-cell stimulatory factor 1, that expresses B-cell- and T-cell-stimulating activities. Proc Natl Acad Sci USA **1986**; 83:5894–8.
30. Bonsch D, Kammer W, Lischke A, Friedrich K. Species-specific agonist/antagonist activities of human interleukin-4 variants suggest distinct ligand binding properties of human and murine common receptor gamma chain. J Biol Chem **1995**; 270:8452–7.
31. Idzerda RL, March CJ, Mosley B, et al. Human interleukin 4 receptor confers biological responsiveness and defines a novel receptor superfamily. J Exp Med **1990**; 171:861–73.
32. Morrison BW, Leder P. A receptor binding domain of mouse interleukin-4 defined by a solid-phase binding assay and in vitro mutagenesis. J Biol Chem **1992**; 267:11957–63.

JOURNAL OF VIROLOGY, July 2008, p. 6762–6766
0022-538X/08/$08.00+0 doi:10.1128/JVI.00018-08

Vol. 82, No. 13

Structural Analysis of Human Immunodeficiency Virus Type 1 CRF01_AE Protease in Complex with the Substrate p1-p6[▽]

Rajintha M. Bandaranayake,[1] Moses Prabu-Jeyabalan,[1] Junko Kakizawa,[2] Wataru Sugiura,[2] and Celia A. Schiffer[1]*

Department of Biochemistry and Molecular Pharmacology, University of Massachusetts Medical School, 364 Plantation Street, Worcester, Massachusetts 01605,[1] and Laboratory of Therapeutic Research and Clinical Science, AIDS Research Center, National Institute of Infectious Diseases, 4-7-1 Gakuenn Musashimurayama, Tokyo 208-0011, Japan[2]

Received 3 January 2008/Accepted 16 April 2008

The effect of amino acid variability between human immunodeficiency virus type 1 (HIV-1) clades on structure and the emergence of resistance mutations in HIV-1 protease has become an area of significant interest in recent years. We determined the first crystal structure of the HIV-1 CRF01_AE protease in complex with the p1-p6 substrate to a resolution of 2.8 Å. Hydrogen bonding between the flap hinge and the protease core regions shows significant structural rearrangements in CRF01_AE protease compared to the clade B protease structure.

Based on its genomic diversity, the human immunodeficiency virus type 1 (HIV-1) has been classified into three groups, M (major), N (nonmajor), and O (other/outlier) (16). Group M has been further defined into nine clades (clades A to D, F to H, and J and K) and a number of subclades and circulating recombinant forms (CRFs). HIV-1 protease is one of the major proteins targeted for anti-HIV drug development. The *pol* gene, which codes for protease, differs by 10 to 15% between clades (7), and sequence diversity within HIV-1 clades has been an important area of study in recent years due to its possible role in altering resistance pathways within the protease (1, 10). In particular, the HIV-1 CRF01_AE protease acquires nelfinavir resistance via an alternative mutational pathway (1), making the detailed study of non-B proteases strongly warranted.

Structural studies of clade B protease have led to the successful development of a number of protease inhibitors (PIs). However, the majority of HIV-1 infection cases in the world result from non-clade B variants, and there is limited evidence that non-clade B variants respond differently to currently available PIs (3, 23). Although a large number of clade B protease structures have been solved over the years, to date, very little structural information is available for non-B HIV proteases. The first non-clade B protease structures for clade F were published recently by Sanches et al. (18), and the crystallization of clade C PI complexes has been reported by Coman et al. (4). We present here the crystal structure of an inactive HIV-1 CRF01_AE protease variant (D25N) in complex with a decameric peptide corresponding to the p1-p6 cleavage site within the Gag and Gag-Pro-Pol polyproteins. CRF01_AE was one of the first CRFs to be identified and is now the predominant HIV-1 variant in Southeast Asia (12). The protease was derived from a Japanese patient isolate and has 10 amino acid substitutions (R14K, K20R, E35D, M36I, R41K, P63I, V64I, H69K, L89M, and I93L) compared to that of clade B (Fig. 1A and B).

Crystallization and structure determination. The CRF01_AE protease was expressed and purified as previously described (14). The protein was concentrated to 1.8 mg ml^{-1} using a 10-kDa molecular size limit Amicon Ultra-15 centrifugal filter device. The decameric p1-p6 peptide (Arg-Pro-Gly-Asn-Phe-Leu-Gln-Ser-Arg-Pro; Quality Controlled Biochemicals, Inc., Hopkinton, MA) was solubilized in dimethyl sulfoxide and equilibrated with the protein with a fivefold molar excess for 1 h on ice. Crystals were grown over a reservoir solution consisting of 126 mM phosphate buffer at pH 6.2 and 63 mM sodium citrate and ammonium sulfate in the range of 18 to 33% (20). A 2:1 volume ratio of reservoir solution and substrate-protein solution were combined to set up hanging drops with a final volume of 6 μl. The crystals were grown at ambient temperature.

Crystallographic data were collected under cryogenic conditions using an R-AXIS IV image plate mounted on a Rigaku rotating anode X-ray generator. The data were reduced and scaled using the programs DENZO and SCALEPACK, respectively (13). Structure determination and refinement were carried out using programs within the CCP4 software suite as previously described (15). Model building was carried out, followed by real space refinement with the COOT molecular graphics software (5). Refinement of the initial models was done without the p1-p6 substrate, and the peptide was built into the $F_o - F_c$ density within the active site as the refinement progressed. A truncated p1-p6 peptide lacking ArgP5 and ProP4 was modeled into the active site, as the $2Fo-Fc$ and $Fo - Fc$ maps indicated weak and discontinuous electron density at the N terminus of the peptide. The ArgP4′ of the p1-p6 peptide was modeled in as alanine, since the electron density was not well defined to model in the arginine side chain. The stereochemical parameters of the final model were checked using PROCHECK (11). The CRF01_AE protease in complex

* Corresponding author. Mailing address: Department of Biochemistry and Molecular Pharmacology, University of Massachusetts Medical School, 364 Plantation Street, Worcester, MA 01605. Phone: (508) 856-8008. Fax: (508) 856-6464. E-mail: Celia.Schiffer@umassmed.edu.
▽ Published ahead of print on 23 April 2008.

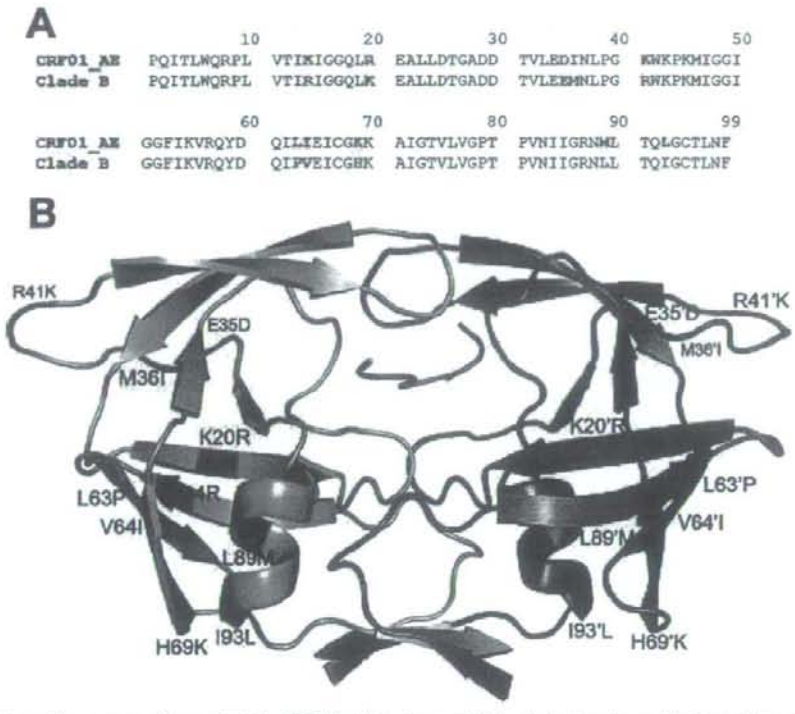

FIG. 1. (A) Amino acid sequence alignment of the CRF01_AE protease with the clade B protease. Positions where sequences differ are indicated in red. (B) CRF01_AE protease in complex with p1-p6 (green). Amino acid changes in monomer A (cyan) are indicated in red, and changes in monomer B (magenta) are indicated in blue.

TABLE 1. Crystallographic data and statistics for CRF01_AE in complex with substrate p1-p6

Parameter	Value
Resolution (Å)	2.8
Temperature (°C)	Cryogenic
Space group	$P6_1$
Cell dimensions	
a = b (Å)	62.1
c (Å)	82.1
Z'	6
R_{merge} (%)	9.5
Completeness (%)	99.4
Total no. of reflections	45,495
No. of unique reflections	4,523
I/σ^I	8.4
RMSD in[b]	
Bond lengths (Å)	0.008
Bond angles (Å)	1.2
R_{factor} (%)	19.9
R_{free} (%)	25.8

[a] Number of molecules in the unit cell.
[b] RMSD, root-mean-square deviation.

with p1-p6 was determined to a resolution of 2.8 Å (PDB code 3D3T) (Table 1).

Protease structure comparison. The clade B D25N protease in complex with p1-p6 (PDB code 1KJF) was used for structural comparisons. The terminal regions (residues 1 to 9 and 86 to 99) from both monomers were used to superimpose the clade B structure onto the CRF01_AE complex. The superimposition was performed in a way that preserved the orientation of the substrate peptide between the two structures. A double-difference plot was generated to visualize structural differences between the two complexes. Distances between all the Cα atoms within the dimer were calculated for each complex, and then the difference of the difference between the two dimers was plotted as a contour plot, as previously described (15). The presence of significant contour peaks within the plot indicates regions that differ between the two structures.

Based on the Cα superimposition, the CRF01_AE and clade B structures displayed a high level of structural similarity to each other, with a root-mean-square deviation of 0.37 Å (Fig. 2A). However, peaks within the double-difference plot show that the CRF01_AE complex has significant structural rearrangements at the flap hinge region (residues 33 to 39) and near the protease core region (residues 16 to 22) (Fig. 2B). These structural differences are present in both monomers of the complex. Closer examination of Ile36 shows that its shorter

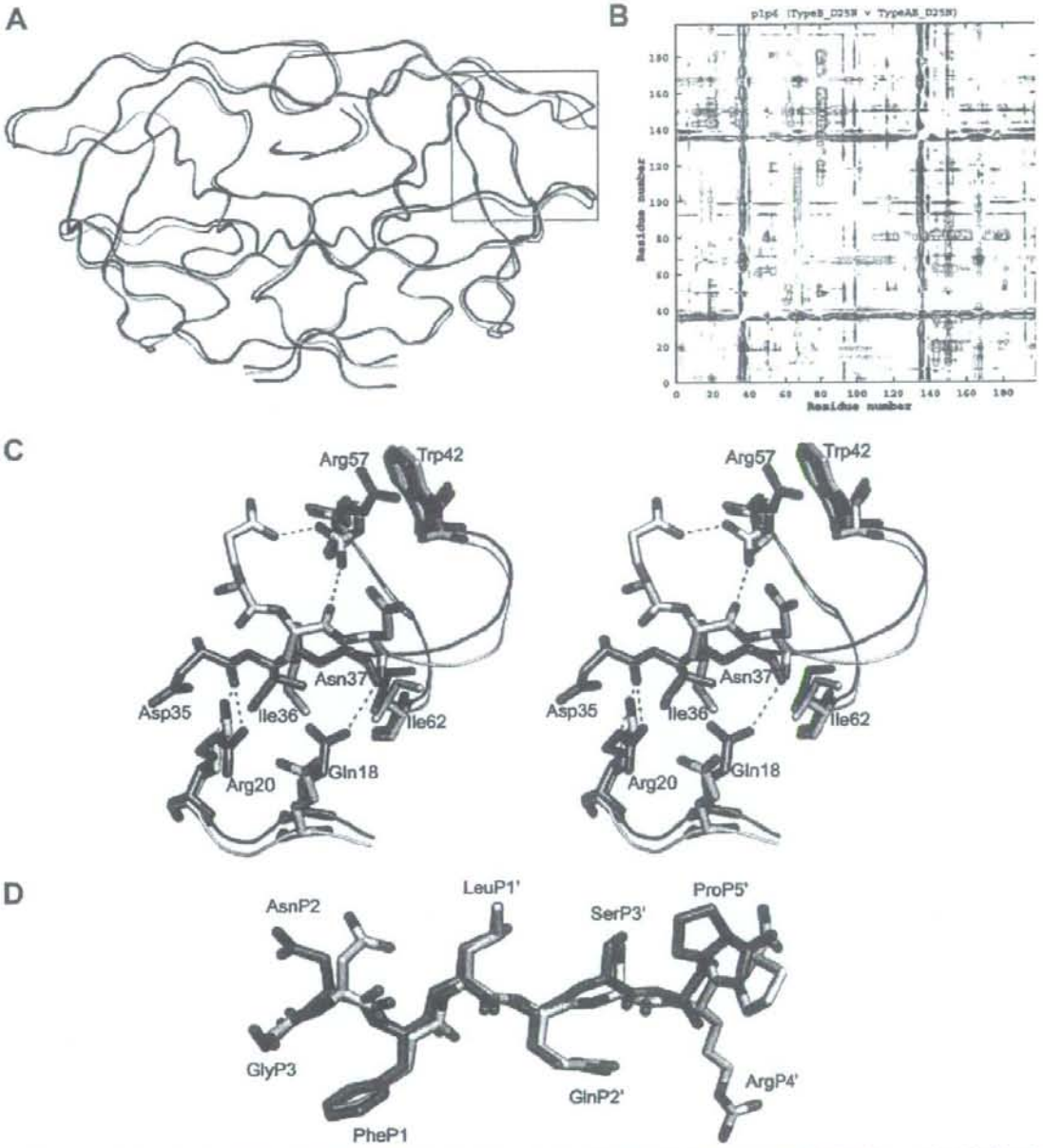

FIG. 2. (A) Ribbon diagram superposition of the CRF01_AE (blue) and the clade B (gray) p1-p6 structures. The flap hinge region is indicated by the red box. (B) Double-difference plot comparing the CRF01_AE and clade B p1-p6 structures. Contours in the plot represent the degrees of distance between the residues of the structures being compared. Black indicates a distance of <0.6 Å; red indicates −0.59 Å and −0.3 Å; blue indicates 0.3 Å and 0.59 Å; and yellow indicates >0.6 Å. (C) Stereoview of the rearrangement of the flap hinge region of the CRF01_AE structure (blue) compared to that of the clade B structure (gray). The Asn37 side chain in the CRF01_AE structure is disordered and has been modeled as alanine. (D) p1-p6 substrate conformation (blue, CRF01_AE; gray, clade B).

TABLE 2. Substrate-protease hydrogen bonds

Substrate atom	Protease atom	Distance (Å) between[a]:	
		CRF01_AE protease	Clade B protease
GlyP3 N	Gly48 O	3.5	3.0
GlyP3 O	Asp29 N	3.0	2.8
AsnP2 OD-1	Asp29 N	**2.8**	
AsnP2 OD-1	Asp30 N	**2.8**	
AsnP2 ND-2	Asp30 OD2	**3.1**	
PheP1 N	Gly27 O	2.6	2.9
PheP1 O	Asn25 ND2	2.8	2.7
GlnP2′ N	Gly27′ O	2.9	3.0
GlnP2′ OE-1	Asp29′ N	3.1	2.9
GlnP2′ OE-1	Asp30′ N	2.7	2.7
GlnP2′ NE-2	Asp30′ OD2	2.6	3.0
GlnP2′ O	Asp29′ N	2.8	3.1
Gln P2′ OE-1	Asp30′ OD2	3.4	3.3
SerP3′ OG	Asp29′ OD2	2.8	3.4
SerP3′ OG	Arg8 NH1	**3.1**	
SerP3′ N	Gly48′ O	3.1	3.0
SerP3′ O	Gly48′ N	3.2	2.8
ArgP4′ NE	Asp30′ OD1	NA[b]	3.2
ArgP4′ NE	Asp30′ OD2	NA[b]	3.0
ArgP4′ NH-2	Gln58′ OE1	NA[b]	3.4

[a] Distances highlighted in bold are hydrogen bonds that are observed only in the CRF01_AE structure.
[b] Distances are not available (NA) as the ArgP4′ side chain is disordered.

side chain is stabilized through van der Waals interactions with the side chains of Asn18, Leu38, and Arg20, allowing the flap hinge region to pack closer to the core region when compared to the longer Met36 side chain in the clade B structure (Fig. 2C). The collapse of the flap hinge toward the core is further enhanced by the formation of a hydrogen bond between the carbonyl oxygen of Asp35 and the NE or NH-2 of the Arg20 side chain. This interaction causes the Asp35 side chain to flip inward toward the core region. In comparison, the longer Glu35 side chain in clade B is flipped outward into the solvent, allowing its OE-2 oxygen to form a hydrogen bond with the side chain NH-1 of Arg57. The positioning of the Arg57 side chain also allows the NH-2 hydrogen to form a hydrogen bond with the carbonyl oxygen of Met36. The Arg57 side chain of the CRF01_AE structure is not involved in making any interactions with the flap hinge and packs against Trp42. These observations suggest that the flap hinge region of the CRF01_AE protease is likely to have reduced flexibility as a result of its tighter packing against the protease core region than against clade B.

Substrate conformation. The p1-p6 peptide is bound within the active site in an extended conformation with the Phe-Leu cleavage site at positions P1 and P1′, oriented between the "catalytic" Asn25 residues. AsnP2 in the CRF01_AE structure adopts a conformation different from that of the clade B structure (Fig. 2D). OG of SerP3′ also adopts an orientation that is different from that seen in the clade B structure. ProP5′ is rotated by 180°, which causes the C terminus of the peptide to kink toward the P4′ position, whereas in the clade B complex, the p1-p6 peptide adopts an extended conformation at the C terminus. Despite changes in peptide conformation, the protease-substrate hydrogen bonding patterns show a high degree of similarity between the two structures, with 13 substrate-protease hydrogen bonds conserved between the CRF01_AE and the clade B structures (Table 2). However, the CRF01_AE structure makes four additional substrate-protease hydrogen bonds that are not seen in the clade B structure. The AsnP2 side chain conformation allows OD-1 to form a hydrogen bond with either Asp29 N or Asp30 N, while ND-2 forms a hydrogen bond with Asp30 OD-2. Furthermore, the AsnP2 side chain confirmation allows it to make significant van der Waals interactions with Asp29 and Asp30. The hydrogen bond formed between SerP3′ OG and Arg8 NH_1 is a result of SerP3′ OG adopting an orientation that is different from that seen in the clade B structure. Thus, compared to the clade B structure, the p1-p6 substrate appears to form better interactions with the CRF01_AE active site.

Conclusions. The structure described in this study is the first CRF01_AE protease structure, as well as the first non-B HIV-1 protease-substrate complex structure, to be reported to date. The R20, D35, I36, K69, M89, and L93 seen in the structure have been implicated as resistance-associated mutations in clade B protease (2, 8, 9). While no significant structural changes were observed at K69, M89, and L93, the R20, D35, and I36 substitutions in the CRF01_AE protease resulted in significant structural rearrangements of the flap hinge and core regions compared to that in the clade B structure. We have observed a similar structural rearrangement in a CRF01_AE protease structure in an inhibitor complex (unpublished data), which might be an indication that the interactions observed are unique to the CRF01_AE protease.

Movement of the flaps is essential for substrate binding, and the flap hinge and core regions play key roles in flap dynamics (17, 19, 21). The close packing observed between these regions in the CRF01_AE protease structure is likely to restrict flexibility and thereby affect flap dynamics. The protease molecule itself undergoes large conformational changes in order to facilitate substrate binding and product release following substrate cleavage (6). Thus, reduced flexibility resulting from the packing of the flap hinge and core regions may have an effect on protease activity as well. Previously reported enzyme kinetics data for a CRF01_AE variant indicate that the active site specificity and catalytic efficiency are slightly lower for the CRF01_AE protease than for the clade B protease (3). Furthermore, polymorphisms occurring within these regions are thought to affect binding affinities for PIs (22). Therefore, the structural changes observed may influence how the CRF01_AE protease interacts with PIs and may thereby alter levels of resistance to currently available inhibitors compared to that of clade B protease.

We thank Madhavi Nalam and Balaji Bhyravbhatla for assistance with structural refinement.

This work was supported by National Institutes of Health grant 2R01-GM064347-06.

REFERENCES

1. **Ariyoshi, K., M. Matsuda, H. Miura, S. Tateishi, K. Yamada, and W. Sugiura.** 2003. Patterns of point mutations associated with antiretroviral drug treatment failure in CRF01_AE (subtype E) infection differ from subtype B infection. J. Acquir. Immune Defic. Syndr. **33**:336–342.
2. **Becker-Pergola, G., P. Kataaha, L. Johnston-Dow, S. Fung, J. B. Jackson, and S. H. Eshleman.** 2000. Analysis of HIV type 1 protease and reverse transcriptase in antiretroviral drug-naive Ugandan adults. AIDS Res. Hum. Retrovir. **16**:807–813.
3. **Clemente, J. C., R. M. Coman, M. M. Thiaville, L. K. Janka, J. A. Jeung, S. Nukoolkarn, L. Govindasamy, M. Agbandje-McKenna, R. McKenna, W. Leelamanit, M. M. Goodenow, and B. M. Dunn.** 2006. Analysis of HIV-1

CRF_01 A/E protease inhibitor resistance: structural determinants for maintaining sensitivity and developing resistance to atazanavir. Biochemistry **45**: 5468–5477.

4. **Coman, R. M., A. Robbins, M. M. Goodenow, R. McKenna, and B. M. Dunn.** 2007. Expression, purification and preliminary X-ray crystallographic studies of the human immunodeficiency virus 1 subtype C protease. Acta Crystallogr. F **63**:320–323.
5. **Emsley, P., and K. Cowtan.** 2004. Coot: model-building tools for molecular graphics. Acta Crystallogr. D **60**:2126–2132.
6. **Foulkes-Murzycki, J. E., W. R. Scott, and C. A. Schiffer.** 2007. Hydrophobic sliding: a possible mechanism for drug resistance in human immunodeficiency virus type 1 protease. Structure **15**:225–233.
7. **Gonzales, M. J., R. N. Machekano, and R. W. Shafer.** 2001. Human immunodeficiency virus type 1 reverse-transcriptase and protease subtypes: classification, amino acid mutation patterns, and prevalence in a northern California clinic-based population. J. Infect. Dis. **184**:998–1006.
8. **Julg, B., and F. D. Goebel.** 2005. HIV genetic diversity: any implications for drug resistance? Infection **33**:299–301.
9. **Kantor, R., and D. Katzenstein.** 2003. Polymorphism in HIV-1 non-subtype B protease and reverse transcriptase and its potential impact on drug susceptibility and drug resistance evolution. AIDS Rev. **5**:25–35.
10. **Kantor, R., D. A. Katzenstein, B. Efron, A. P. Carvalho, B. Wynhoven, P. Cane, J. Clarke, S. Sirivichayakul, M. A. Soares, J. Snoeck, C. Pillay, H. Rudich, R. Rodrigues, A. Holguin, K. Ariyoshi, M. B. Bouzas, P. Cahn, W. Sugiura, V. Soriano, L. F. Brigido, Z. Grossman, L. Morris, A. M. Vandamme, A. Tanuri, P. Phanuphak, J. N. Weber, D. Pillay, P. R. Harrigan, R. Camacho, J. M. Schapiro, and R. W. Shafer.** 2005. Impact of HIV-1 subtype and antiretroviral therapy on protease and reverse transcriptase genotype: results of a global collaboration. PLoS Med. **2**:e112.
11. **Laskowski, R. A., M. W. Mac Arthur, D. S. Moss, and J. M. Thornton.** 1993. PROCHECK. A program to check the stereochemical quality of protein structures. J. Appl. Crystallogr. **26**:283–291.
12. **McCutchan, F. E.** 2006. Global epidemiology of HIV. J. Med. Virol. **78**(Suppl. 1):S7–S12.
13. **Otwinowski, Z., and W. Minor.** 1997. Processing of X-ray diffraction data collected in oscillation mode. Methods Enzymol. **276**:307–326.
14. **Prabu-Jeyabalan, M., E. Nalivaika, N. M. King, and C. A. Schiffer.** 2004. Structural basis for coevolution of the human immunodeficiency virus type 1 nucleocapsid-p1 cleavage site with a V82A drug-resistant mutation in viral protease. J. Virol. **78**:12446–12454.
15. **Prabu-Jeyabalan, M., E. A. Nalivaika, K. Romano, and C. A. Schiffer.** 2006. Mechanism of substrate recognition by drug-resistant human immunodeficiency virus type 1 protease variants revealed by a novel structural intermediate. J. Virol. **80**:3607–3616.
16. **Robertson, D. L., J. P. Anderson, J. A. Bradac, J. K. Carr, B. Foley, R. K. Funkhouser, F. Gao, B. H. Hahn, M. L. Kalish, C. Kuiken, G. H. Learn, T. Leitner, F. McCutchan, S. Osmanov, M. Peeters, D. Pieniazek, M. Salminen, P. M. Sharp, S. Wolinsky, and B. Korber.** 2000. HIV-1 nomenclature proposal. Science **288**:55–56.
17. **Rose, R. B., C. S. Craik, and R. M. Stroud.** 1998. Domain flexibility in retroviral proteases: structural implications for drug resistant mutations. Biochemistry **37**:2607–2621.
18. **Sanches, M., S. Krauchenco, N. H. Martins, A. Gustchina, A. Wlodawer, and I. Polikarpov.** 2007. Structural characterization of B and non-B subtypes of HIV-protease: insights into the natural susceptibility to drug resistance development. J. Mol. Biol. **369**:1029–1040.
19. **Scott, W. R., and C. A. Schiffer.** 2000. Curling of flap tips in HIV-1 protease as a mechanism for substrate entry and tolerance of drug resistance. Structure **8**:1259–1265.
20. **Silva, A. M., R. E. Cachau, H. L. Sham, and J. W. Erickson.** 1996. Inhibition and catalytic mechanism of HIV-1 aspartic protease. J. Mol. Biol. **255**:321–346.
21. **Todd, M. J., and E. Freire.** 1999. The effect of inhibitor binding on the structural stability and cooperativity of the HIV-1 protease. Proteins **36**:147–156.
22. **Velazquez-Campoy, A., M. J. Todd, S. Vega, and E. Freire.** 2001. Catalytic efficiency and vitality of HIV-1 proteases from African viral subtypes. Proc. Natl. Acad. Sci. USA **98**:6062–6067.
23. **Velazquez-Campoy, A., S. Vega, and E. Freire.** 2002. Amplification of the effects of drug resistance mutations by background polymorphisms in HIV-1 protease from African subtypes. Biochemistry **41**:8613–8619.

THE JOURNAL OF BIOLOGICAL CHEMISTRY VOL. 284, NO. 6, pp. 3513–3520, February 6, 2009

A Single Amino Acid of Toll-like Receptor 4 That Is Pivotal for Its Signal Transduction and Subcellular Localization*

Received for publication, April 22, 2008, and in revised form, October 29, 2008 Published, JBC Papers in Press, December 8, 2008, DOI 10.1074/jbc.M803086200

Shintaro Yanagimoto[‡§¶], Keita Tatsuno[§], Shu Okugawa[§], Takatoshi Kitazawa[§], Kunihisa Tsukada[§], Kazuhiko Koike[§], Tatsuhiko Kodama[¶], Satoshi Kimura[‖], Yoshikazu Shibasaki[‡1], and Yasuo Ota[1,2]**

From the [‡]Center for Structuring Life Sciences, Graduate school of Arts and Sciences, University of Tokyo, Meguro-ku, Tokyo 153-8903, the [§]Department of Infectious Diseases, Graduate School of Medicine, University of Tokyo, Bunkyo-ku, Tokyo 113-8655, the [¶]Laboratory for Systems Biology and Medicine, Research Center for Advanced Science and Technology, University of Tokyo, Meguro-ku, Tokyo 153-8904, the [‖]Tokyo Teishin Hospital, Fujimi, Chiyoda-ku, Tokyo 102-8798, and the [**]Department of Medicine, Teikyo University School of Medicine, 2-11-1, Kaga, Itabashi-ku, Tokyo 173-8605, Japan

Toll-like receptor 4 (TLR4) is essential for recognizing a Gram-negative bacterial component, lipopolysaccharide (LPS). A single amino acid mutation at position 712 of murine TLR4 leads to hyporesponsiveness to LPS. In this study we determined that an amino acid, a leucine at position 815 of human TLR4, is also pivotal for LPS responsiveness and subcellular distribution. By replacing the leucine with alanine, the mutant TLR4 lost responsiveness to LPS and did not localize on the plasma membrane. In addition, it does not coprecipitate with myeloid differentiation-2, an accessory protein that is necessary for TLR4 to recognize LPS. These results suggest that the leucine at position 815 is required for the normal maturation of TLR4 and for formation of the TLR4·MD-2 complex.

Toll-like receptors (TLRs)[3] play essential roles in both innate and adaptive immunity (1). Thirteen members of the TLR family have been identified in mammals. TLRs have leucine-rich-repeats in their extracellular domains and a Toll/Interleukin-1 receptor (TIR) in their cytoplasmic domains, the latter of which mainly mediates intracellular signaling. Signaling pathways of TLRs, except for TLR3, depend on an adapter protein, MyD88 (myeloid differentiation factor 88), which interacts with the TIR domain of TLRs. This pathway leads to the activation of the transcription factor NF-κB and production of cytokines such as tumor necrosis factor-α and interleukin-6. Another important signaling pathway mediated by TLR3 and TLR4 that exploits the TIR domain is the MyD88-independent pathway. This pathway involves different adapter proteins, such as the TIR domain-containing adaptor inducing interferon-β (TRIF) and TRIF-related adaptor molecule (2–4), and is essential for production of type I interferon through activation of interferon regulatory factor-3.

TLRs recognize as ligands several microbial pathogen-associated molecular patterns. One such pathogen-associated molecular pattern is lipopolysaccharide (LPS), which is recognized by TLR4. LPS triggers severe immunologic reactions by the host in Gram-negative bacterial infections and has drawn attention in many clinical situations. TLR4 is the first mammalian TLR to be discovered in the context of immunology. TLR4 was identified in the search for the genes responsible for LPS hyporesponsiveness (5, 6). The defect was found to stem from a single amino acid mutation, replacement of proline with histidine at position 712, in the cytoplasmic tail of murine TLR4. The study led to the discovery of the importance of TLR4 in innate immunity.

A variety of cells are activated by LPS stimulation through TLR4. TLR4 forms a receptor complex with an accessory protein, myeloid differentiation-2 (MD-2). MD-2 first associates with TLR4 in the endoplasmic reticulum (ER) and *cis*-Golgi, and both proteins move together to the plasma membrane (7, 8). Upon recognition of LPS, the TLR4·MD-2 complex receives LPS on the cell surface and initiates intracellular signaling. The expression of TLR4 in the absence of MD-2 does not confer full responsiveness to LPS stimuli in experimental cell lines (9). An analysis of MD-2 knockout mice revealed that MD-2 is important not only for LPS sensing but also for cellular distribution of TLR4.

In this study we hypothesized that the cytoplasmic tail of TLR4 contains regions that control both localization and signaling. Using truncation and mutation analysis, and paying particular attention to the TIR domain, we identified a single amino acid that is pivotal for both TLR4 signaling and subcellular distribution. The site we found was on the C-terminal portion of the TIR domain for which no specific function has been yet determined.

* This work was partly supported by the Program of Fundamental Studies in Health Sciences of the National Institute of Biomedical Innovation, by the Focus 21 project of the New Energy and Industrial Technology Development Organization, and by the Special Coordination Fund for Science and Technology from the Ministry of Education, Culture, Sports, Science and Technology. This study was also partly supported by a grant-in-aid from the Ministry of Education, Culture, Sports, Science and Technology (to Y. O.). The costs of publication of this article were defrayed in part by the payment of page charges. This article must therefore be hereby marked "*advertisement*" in accordance with 18 U.S.C. Section 1734 solely to indicate this fact.

[1] Both authors contributed equally to this work.

[2] To whom correspondence should be addressed. Tel.: 81-3-3964-1211 (ext. 1756); Fax: 81-3-3579-6310; E-mail: yasuota-tky@umin.ac.jp.

[3] The abbreviations used are: TLR, Toll-like receptor; TIR, Toll/Interleukin-1 receptor; TRIF, TIR domain-containing adaptor inducing interferon-β; LPS, lipopolysaccharide; MD-2, myeloid differentiation-2; ER, endoplasmic reticulum; GFP, green fluorescent protein; EGFP, enhanced GFP; RLA, relative luciferase activity; Sulfo-NHS-SS-Biotin, sulfosuccinimidyl-2-(biotinamido)ethyl-1,3-dithiopropionate.

EXPERIMENTAL PROCEDURES

Reagents and Other Materials—Lipopolysaccharide (LPS) from *Escherichia coli* O55:B5 was purchased from Sigma-Aldrich and applied without repurification. FLAG- and hexa-histidine (His_6)-tagged human TLR4 expression plasmid (pEFBOS/humanTLR4flaghis) and FLAG- and His_6-tagged human MD-2 expression plasmid (pEFBOS/humanMD-2flaghis) were generous gifts from Dr. Kensuke Miyake (Institute of Medical Science, University of Tokyo, Japan). Human CD14 cDNA plasmid (pCMV6-XL5/humanCD14) was purchased from OriGene (Rockville, MD). Fluorescent protein expression vector pEGFP-N3 was purchased from Clontech (Mountain View, CA). Anti-TLR4 monoclonal antibody (clone HTA125) was purchased from Abcam (Cambridge, MA). Anti-FLAG monoclonal antibody (clone M2) was purchased from Sigma-Aldrich. Anti-*A.v.* (GFP) monoclonal and polyclonal antibodies were purchased from Clontech. Control immunoglobulins for immunoprecipitation were purchased from BD Biosciences (San Jose, CA). Horseradish peroxidase-labeled anti-immunoglobulins antibodies were purchased from Dako (Glostrup, Denmark). BlockAce (DS Pharma Biomedical, Osaka, Japan) solution was used as blocking buffer for Western blotting.

Cell Culture—Human embryonic kidney (HEK) 293T cells were maintained in Dulbecco's modified Eagle's medium (Sigma-Aldrich) containing 10% heat-inactivated fetal bovine serum supplemented with penicillin-streptomycin solution (Invitrogen). FuGENE 6 transfection reagent (Roche Applied Science) was used for transient cotransfection according to the manufacturer's instructions. Culture dishes or plates were prepared to 70% confluence prior to transfection. Cells were used for experiments 36 h later. The transfection conditions were optimized for microscopic observation of the expressed fluorescent protein and were kept unchanged in other experiments.

Expression Vector Subcloning and Mutagenesis—Wild-type TLR4 cDNA was excised from pEFBOS/humanTLR4flaghis and subcloned into pEGFP-N3 so that when expressed enhanced green fluorescent protein (EGFP) would be fused at the C terminus of TLR4 (pEGFP-N3/humanTLR4). All mutations were introduced into pEFBOS/humanTLR4flaghis and pEGFP-N3/humanTLR4 using the QuikChange site-Directed mutagenesis kit (Stratagene, La Jolla, CA) according to the manufacturer's instructions and were confirmed by sequencing. For the truncation analysis, two identical unique restriction sites were prepared in the TLR4-coding region of pEFBOS/humanTLR4 using a QuikChange kit, and the DNA fragment to be removed, which was a part of the C terminus of TLR4, was excised enzymatically. After agarose gel purification, the linear double-stranded DNA was ligated to re-form a circular plasmid. Restriction sites were designed so as not to cause a frameshift between TLR4 and EGFP.

Confocal Laser Scanning Microscopy of Cells—Samples were fixed in 3% paraformaldehyde-phosphate-buffered saline at 37 °C for 10 min. Fluorescence images of fixed samples were recorded using a FluoView FV1000 Confocal Microscope (an inverted confocal laser scanning microscope, Olympus, Tokyo, Japan).

Immunoprecipitation—Transfected cells were lysed in lysis buffer (50 mM Tris-HCl, pH 7.5, 100 mM NaCl, 0.1% Triton X-100, 1 mM 1,4-dithiothreitol, and proteinase inhibitor mixture), sonicated, and centrifuged at 4 °C. Antibody was added to the supernatant, and the sample was rotated 1 h at 4 °C followed by the addition of protein G-Sepharose (GE Healthcare Life Sciences, Piscataway, NJ) and an additional 8-h incubation at 4 °C. Bound protein was washed three times in lysis buffer. Proteins were eluted by boiling in SDS sample buffer.

Biotinylation and Purification of Cell Surface Proteins—Prior to surface biotinylation, HEK 293T cells plated in a 100-mm dish were transiently transfected as described above. Surface biotinylation and subsequent purification of biotinylated proteins were performed using a Cell Surface Protein Biotinylation and Purification Kit (Pierce) following the manufacturer's instructions. Briefly, membrane-impermeable sulfosuccinimidyl-2-(biotinamido)ethyl-1,3-dithiopropionate (Sulfo-NHS-SS-Biotin) was added to cell monolayers in the culture dishes and covalently bound to amines in proteins exposed on the cell surface. The affinity resin that binds to the biotin end of Sulfo-NHS-SS-Biotin was used to collect the biotinylated proteins. Reduction by 1,4-dithiothreitol causes cleavage of the disulfide bond in Sulfo-NHS-SS-Biotin, and the elute contains the biotinylated cell surface proteins. Each final sample obtained was considered to contain proteins from an equal amount of cells, because all culture plates were treated equally and grown to full confluence. All samples were sonicated and subjected to SDS-PAGE and Western blotting. The membrane to which protein was transferred was blocked in blocking buffer for 1 h. Then the membrane was incubated with a primary antibody, followed by incubation with horseradish peroxidase-labeled anti-immunoglobulins antibody. The protein bands were then visualized by using a chemiluminescence reagent, Immobilon Western Chemiluminescent HRP Substrate (Millipore, Billerica, MA), according to the manufacturer's instructions.

Cell Stimulation Assays—HEK293T cells were plated and transiently transfected for assays. Thirty-six hours after the transfection, LPS was added to fresh culture medium in each well of the culture plates at the stated concentration. The duration of LPS stimulation was 7 h.

Dual Luciferase Reporter Assays for NF-κB Activation—HEK293T cells were plated in 12-well culture plates (4×10^4 cells/well), and experimental cDNA plasmids were transiently transfected 36 h later using the FuGENE 6 transfection reagent with 0.5 μg of NF-κB reporter plasmid expressing firefly luciferase (pNF-κB-Luc, Stratagene) and 0.05 μg of constitutively active *Renilla* luciferase reporter plasmid (pRL-TK, Promega, Madison, WI) in addition to 0.5 μg each of TLR4-EGFP plasmid and MD-2 plasmid. Stimulation experiments were performed 36 h later. Firefly luciferase and *Renilla* luciferase activities were measured using the Dual-Luciferase Reporter Assay System (Promega) and the Genelight55 luminometer (Microtech, Chiba, Japan). Relative luciferase activity (RLA) was obtained as the ratio of firefly luciferase activity to *Renilla* luciferase activity. Results are expressed as the ratio of RLA with LPS stimulation to RLA without LPS stimulation ([RLA LPS+]/[RLA LPS−]). This ratio should ideally approach 1 when no response to LPS stimulation is observed.

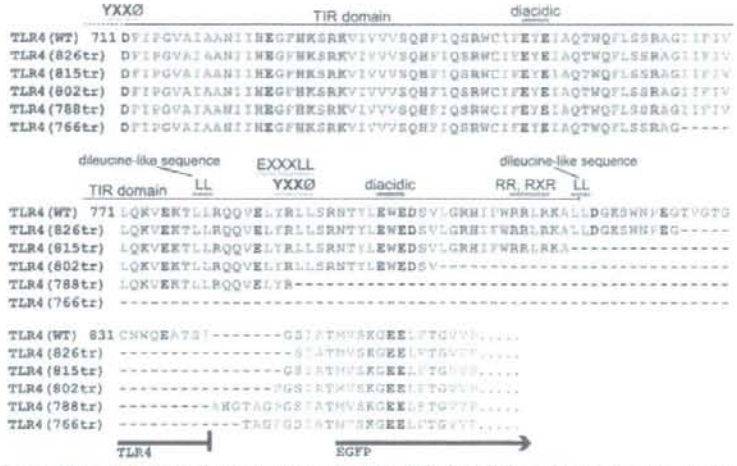

FIGURE 1. **Alignment of the cytoplasmic domains of EGFP fusion TLR4 truncation mutants used in this study.** TLR4 (766tr) signifies the mutant truncated at position 766. Others are named in the same manner. The amino acids are colored based on their physicochemical properties: *pink*, basic; *blue*, acidic; *green*, polar and neutral; and *orange*, hydrophobic. The *black overline* represents the TIR domain. *Colored overlines* indicate amino acid sequences identical to known sorting signal motifs except for two LLs, which are dileucine motif-like sequences in that they consist of solely two consecutive leucines without preceding aspartate or glutamate. *Capital letters* on the *line* signify the single-letter code for amino acids: *E*, glutamic acid; *L*, leucine; *R*, arginine; and *Y*, tyrosine. *X* signifies any amino acid, and Ø signifies an amino acid residue with a bulky hydrophobic side chain.

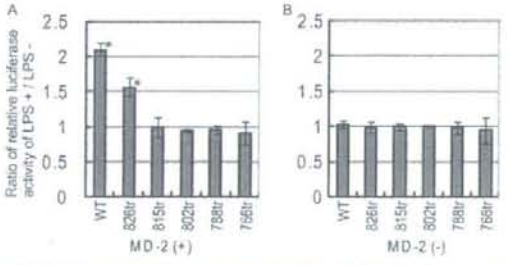

FIGURE 2. **LPS responsiveness measured by NF-κB luciferase assay.** HEK293T cells were transfected with plasmids containing the gene for wild-type TLR4 or a truncated human TLR4-EGFP fusion protein, in addition to a luciferase reporter and human MD-2 plasmid (*A*) or unmodified plasmids (control) (*B*). After 36 h, cells were stimulated with LPS (10 ng/ml) for 7 h, and luciferase reporter gene activity was measured. All results were expressed as the ratio of relative luciferase activity with LPS stimulation to that without stimulation. The data were from three independent experiments. *Small bars* indicate 95% confidence intervals of the mean (p values for * are: TLR4 (WT)-EGFP/MD-2 (+), $p = 0.002$; TLR4 (826tr)-EGFP/MD-2 (+), $p = 0.016$).

Statistical Analyses—All quantitative experiments were repeated three times, and each experiment was done in triplicate. The ratio of relative luciferase activity of LPS+ to LPS− was calculated as the index of the responsiveness to the stimuli as explained above. When positive response is observed, the ratio should significantly exceed one. The means of the ratio were represented in *bar graphs*. The 95% confidence interval of the mean of the ratio was calculated and indicated on each *bar* in the *graph*, and p values were calculated using Student's t distribution compared with the hypothetical mean, one.

RESULTS

Truncation Analysis of TLR 4—To identify amino acid sequences in the cytoplasmic tail of TLR4 that are involved in both signal transduction and subcellular distribution, first we generated five truncation mutants of TLR4 with a fluorescent protein (EGFP) at the C terminus of TLR4.

Although there are no known definite sorting signal motifs in the cytoplasmic tail of TLR4, some amino acid sequences are similar or identical to known general sorting signal motifs as shown in Fig. 1. *YXXØ*, a form of tyrosine-based sorting signal, and *EXXXLL*, a form of dileucine (LL)-based sorting signal, both control protein internalization, lysosomal targeting, and basolateral targeting (10), where "*X*" represents any amino acid, "*Ø*" stands for an amino acid residue with a bulky hydrophobic side chain, and other letters are single-letter abbreviations for the amino acids. "Diacidic" signals such as *DXE* mediate export from the ER (11). *RR* or *RXR* is another example of an ER export signal (12). Truncation sites were chosen so that some of these amino acid sequences were deleted in each mutant. Because the TIR domain, which is essential in TLR4 signaling and possibly subcellular localization (13), spans most of the cytoplasmic domain of TLR4, four out of five mutants have involvement in the TIR domain, which we hypothesized could result in impaired signal transduction and a change in subcellular distribution. Part of the cytoplasmic portion of the amino acid sequence of the truncation mutants is shown in Fig. 1. The five truncation mutant proteins lost their C-terminal tails at positions 826, 815, 802, 788, and 766, respectively, and were conjugated with EGFP *in vitro*. Actual truncation and ligation sites of all actual mutants were confirmed to have the designed DNA alignment by sequencing.

We utilized the luciferase reporter assay to assess NF-κB transcription activity as an indicator of TLR4 response to LPS stimuli. MD-2 is reported to be essential for this response (9). However, because it is not known whether MD-2 is necessary for transduction of the truncated TLR4 signal as well, we performed the assays with and without MD-2. The index of cell responsiveness to the stimulation was measured as the ratio between RLA with LPS stimulation and RLA without LPS stimulation. Only cells transfected with TLR4 (826tr)-EGFP in combination with MD-2 retained responsiveness to LPS stimulation. One exception was wild-type TLR4-EGFP (Fig. 2*A*). HEK293T cells transfected with TLR4 but without MD-2 did not respond to LPS stimuli regardless of the TLR4-EGFP genotype (Fig. 2*B*).

Next, we compared the localization of wild-type and truncated mutants of TLR4-EGFP in HEK293T by fluorescence microscopy (Fig. 3*A*). The wild-type TLR4 cotransfected with MD-2 was expressed on the plasma membrane and also in the

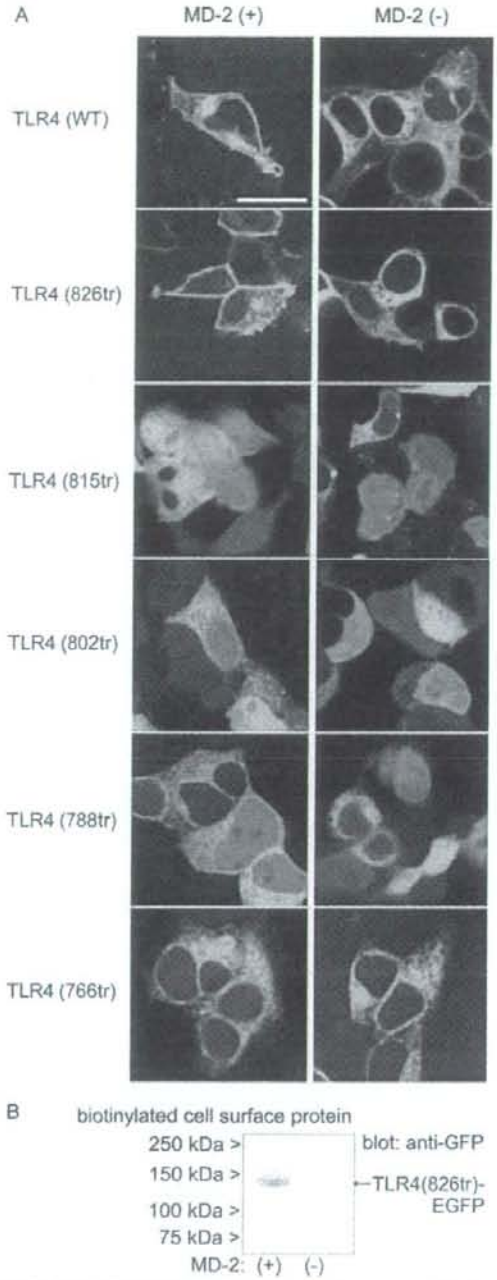

FIGURE 3. **Residues 815–826 of TLR4 contain a region necessary for plasma membrane localization.** *A*, cells were cultured on coverslips in 12-well plates and transfected as in Fig. 2. EGFP-tagged TLR4 was visualized by laser confocal microscopy. Fluorescence from EGFP was observed in *green*. Each genotype of TLR4-EGFP was cotransfected with a human MD-2 plasmid or empty vector. *Bar*, 20 μm. *B*, TLR4 (826tr)-EGFP with or without coexpression of MD-2 were tagged by biotinylation of the cell surface proteins and affinity-purified. TLR4 was visualized by immunoblotting using an anti-GFP monoclonal antibody. Samples from both combinations of DNAs were prepared from the same number of cells.

perinuclear area. These findings were consistent with observations by others (14, 15). TLR4 is reported to localize in the Golgi apparatus as well as on the plasma membrane. Our observation of TLR4-EGFP accumulation in the perinuclear area does not contradict the report that TLR4 partly localizes in the Golgi apparatus (14).

TLR4-EGFP truncation mutants, 815tr, 802tr, 788tr, and 766tr apparently did not localize at the plasma membrane. No particular fluorescence pattern that might be characteristic of localization to a specific intracellular compartment was observed. Only TLR4 (826tr)-EGFP, which has the shortest truncation, was expressed on the plasma membrane and in the perinuclear area, and the fluorescence pattern was similar to that of wild-type (Fig. 3*A*). No TLR4 genotypes, including wild-type TLR4-EGFP, clearly localized on the plasma membrane in the absence of MD-2 (Fig. 3*A*). MD-2 is reported to be necessary for localization of wild-type TLR4 at the plasma membrane (15), which is consistent with our observation. Intracellular distribution of mutant TLR4 varied depending on the genotype, but no particular cellular structure was identified as an alternative target site. Furthermore, we examined the plasma membrane expression of TLR4 (826tr)-EGFP by cell surface protein biotinylation. The expression level of TLR4 (826tr)-EGFP was markedly decreased without coexpression of MD-2 (Fig. 3*B*), which is compatible with the microscope observation.

Removal of the C-terminal segment of TLR4 at residue 826 does not qualitatively affect LPS responsiveness and subcellular distribution. However, when more residues, up to position 815, were removed, both signal transduction and plasma membrane localization were impaired. These results suggest that residues 815–826 of TLR4 contain at least one segment that is critical for those functions.

Amino Acid Sequence Replacement Analysis—To identify critical amino acid sequences in this region, we generated an amino acid replacement mutant of TLR4 instead of truncation mutants. As shown in Fig. 1, although it is not a canonical sequence, leucine-leucine at 815–816 partially fits a known sorting signal motif, a dileucine motif, (D/E)*XXX*(L/I) or D*XX*LL, which plays an important role in internalization of plasma membrane protein or sorting from the *trans*-Golgi network (10). Thus, as has been done in a similar study (16), a mutant was generated in which alanines were substituted for both leucines at positions 815 and 816.

We measured the NF-κB activity of TLR4 (L815AL816A)-EGFP, the mutant in which both leucines were replaced with alanines, under LPS stimulation (Fig. 4*A*). This mutant protein did not respond to LPS stimuli. Microscopic observation revealed that TLR4 (L815AL816A)-EGFP was not expressed on the plasma membrane regardless of whether MD-2 was cotransfected (Fig. 4*B*). The phenotype of this doubly substituted mutant appeared to be the same as that of the truncation mutants. These results imply that the leucines in positions 815 and 816 play an important role in TLR4 plasma membrane localization.

Analysis of Single Amino Acid Substitution Mutants—As previously mentioned, the amino acid sequence leucine-leucine at positions 815 and 816 does not completely match the dileucine motif, *i.e.* it lacks a preceding acidic amino acid. Therefore it

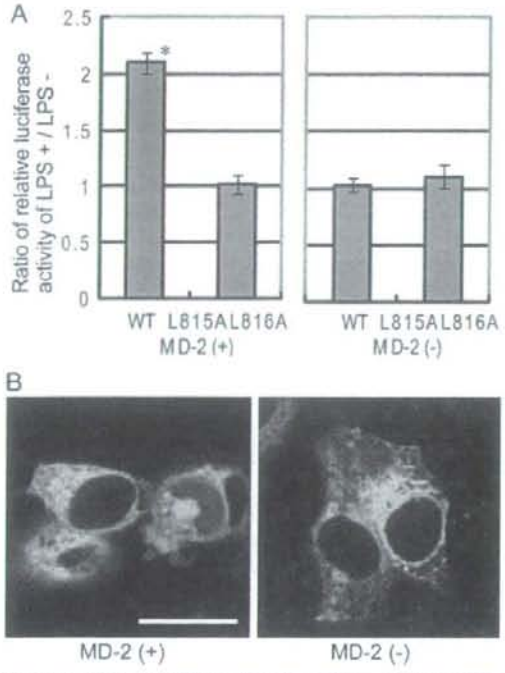

FIGURE 4. **Leucines at positions 815–816 of TLR4 are responsible for impairment of LPS responsiveness and plasma membrane expression.** *A*, the LPS stimulation assay was done for TLR4 (L815AL816A)-EGFP as in Fig. 2. The data were from three independent experiments. *Small bars* indicate 95% confidence intervals of the mean (*p* value for * are: TLR4 (WT)-EGFP/MD-2 (+), $p = 0.002$). *B*, TLR4 (L815AL816A)-EGFP expression in HEK293T cells was observed by laser confocal microscopy. *Bar*, 20 μm.

was reasonable to explore whether leucines 815 and 816 need to be adjacent to each other. We created five genotypes of single amino acid mutants of TLR4: TLR4 (K813A)-EGFP, TLR4 (L815A)-EGFP, TLR4 (L816A)-EGFP, and TLR4 (D817A)-EGFP. We excluded the amino acid at position 814 from the analysis, because the amino acid in position 814 of wild-type TLR4 is alanine. The amino acid sequence alignment of wild-type TLR4 and the single amino acid replacement mutants is shown in Fig. 5. DNA sequences were confirmed by sequencing.

As was done with truncation mutants, we measured NF-κB activity of wild-type TLR4-EGFP, TLR4 (K813A)-EGFP, TLR4 (L815A)-EGFP, TLR4 (L816A)-EGFP, and TLR4 (D817A)-EGFP in response to LPS stimulation. All mutants except TLR4 (L815A)-EGFP showed responsiveness to LPS stimulation with coexpression of MD-2 (Fig. 6*A*). Without MD-2, no genotype of TLR4-EGFP responded to LPS stimulation (Fig. 6*B*). LPS stimulation was performed in an identical manner as with truncation mutants.

We analyzed the subcellular distribution of single amino acid mutants of TLR4-EGFP with and without MD-2 coexpression by fluorescence microscopy. TLR4 (K813A)-EGFP and TLR4 (D817A)-EGFP showed a similar fluorescence pattern to the wild-type, which localized at the plasma membrane when coexpressed with MD-2. No genotypes of TLR4-EGFP localized on the plasma membrane without MD-2 (Fig. 7). The cells transfected with TLR4 (L815A)-EGFP coexpressed with MD-2 did not show plasma membrane fluorescent pattern. Also, TLR4 (L815A)-EGFP showed comparatively weaker fluoresce than other mutants, possibly due to lower expression of the protein. Fluorescence of TLR4 (L816A)-EGFP with MD-2 was ambiguous as for the plasma membrane expression. Some kind of membranous structure was observed in the cytoplasmic area, but the intensity of the plasma membrane green fluorescence was obscure. Together with the results from the LPS stimulation experiment, the leucines at positions 815 and 816 are considered to play important roles in signal transduction and/or subcellular distribution of TLR4.

Because EGFP consists of 239 amino acids, which is about one-third the size of the complete TLR4 protein, the experimental results obtained using TLR4-EGFP could have been influenced by the presence of the EGFP fused at the C terminus of TLR4. To rule out this possibility, we tested the functional integrity of both TLR4 (L815A) and TLR4 (L816A) with and without EGFP at the C terminus. Reporter assays were performed under the same conditions except that the shorter tag, FLAG-His_6, which has only 21-amino acid tags at the C terminus, was fused to TLR4 in place of EGFP. There was no difference

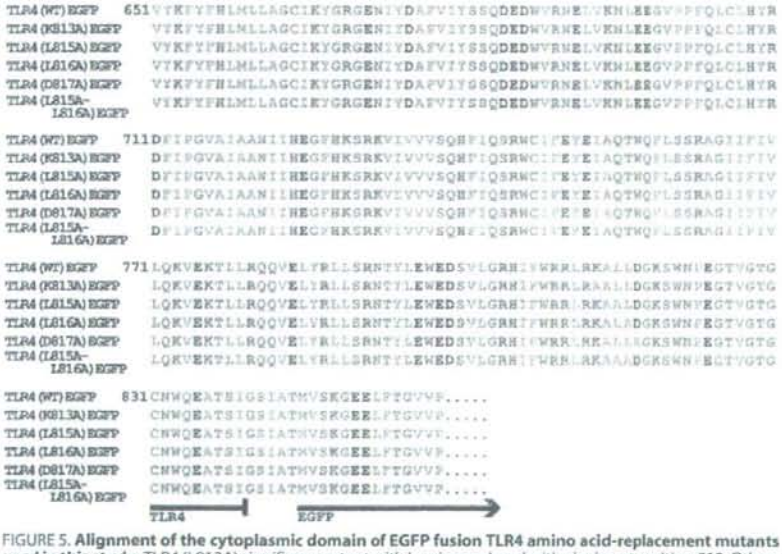

FIGURE 5. **Alignment of the cytoplasmic domain of EGFP fusion TLR4 amino acid-replacement mutants used in this study.** TLR4 (L813A) signifies a mutant with leucine replaced with alanine at position 813. Others are named in the same manner. The amino acids are *colored* as in Fig. 1. All amino acids are designated using the single-letter code.